Amacrine cells shape retinal functions while dynamically preserving circuits for colour vision

Xinwei Wang[1$], Paul A Roberts[1], Takeshi Yoshimatsu[1], Leon Lagnado[1*$] and Tom Baden[1,2*$]

SUMMARY. In vertebrate vision, the feature extracting circuits of the inner retina are driven by heavily pre-processed photoreceptor signals. For example, in larval zebrafish, outer retinal circuits serve to split "colour" from "greyscale" information across their four ancestral cone-photoreceptor types. How then can the inner retina simultaneously preserve such incoming spectral information despite the need to combine cone-signals to shape new greyscale functions?

To address this question, we imaged light-driven signals from the axon terminals of retinal bipolar cells in the presence and pharmacological absence of inhibition from amacrine cells. Surprisingly, this manipulation had no net effect on the inner retinal representation of colour-opponency, despite profound impacts on all tested greyscale functions such as the gain and kinetics of bipolar cell light responses. This 'dynamic balance' was achieved by amacrine cells driving opponency in some bipolar cells, while at the same time suppressing pre-existing opponency in others, such that the net change across the network was essentially zero. To do so, amacrine cells near-exclusively leveraged the On-channel, and correspondingly, a direct *in vivo* survey of amacrine cell functions revealed that all their colour-opponent responses were located in the On-layer. In contrast, Off-stratifying amacrine cells were largely achromatic. We conclude that complex interactions within the inner retina that underlie greyscale visual processing tasks are intricately balanced via the On-channel to not notably alter the pre-existing population representation of colour information.

1, School of Life Sciences, University of Sussex, Biology Road, BN1 9QG, Brighton, UK; 2, Institute of Ophthalmic Research, University of Tübingen, Elfriede-Aulhorn-Strasse 7, 72076, Tübingen, Germany.

[*]Equal contribution, [$]Correspondence to w24@sussex.ac.uk (XW), l.lagnado@sussex.ac.uk (LL), t.baden@sussex.ac.uk (TB).

Twitter: @XinweiWang1017 (XW), @PAR_EyeMath (PAR), @TaYoshimatsu (TY), @Neonsynapse (LL), @NeuroFishh (TB)

Acknowledgements. We thank Thomas Euler for critical feedback. The authors would also like to acknowledge support from the FENS-Kavli Network of Excellence and the EMBO YIP. Funding was provided by the Wellcome Trust (Investigator Award in Science 220277/Z20/Z to TB and 102905/Z/13/Z to LL), the European Research Council (ERC-StG "NeuroVisEco" 677687 to TB), UKRI (BBSRC, BB/R014817/1 to TB), the Leverhulme Trust (PLP-2017-005 and RPG-2021-026 to TB) and the Lister Institute for Preventive Medicine (to TB). This research was funded in whole, or in part, by the Wellcome Trust [220277/Z20/Z and 102905/Z/13/Z to LL]. **For the purpose of Open Access, the authors have applied a CC BY public copyright licence to any Author Accepted Manuscript version arising from this submission.**

Author contributions. Conceptualization, XW, LL, TB; Methodology, XW, PAR, TY; Investigation, XW, PAR; Data Curation, XW, TB; Writing – Original Draft, TB; Writing – Review & Editing, XW, PAR, TY, LL, TB; Visualization, XW, TB; Supervision, LL, TB; Project Administration, LL, TB; Funding Acquisition, LL, TB.

Declaration of Interests. The authors declare no conflict of interest

INTRODUCTION. Animal eyes encode patterns of light along distinct axes of variation such as space, time, and "colour"[1]. These axes combine signals from a shared population of photoreceptors, which poses a general question in neural circuit organisation: how can a common set of inputs be processed such that optimisation for one task does not simultaneously deteriorate function elsewhere?

One strategy is to implement different processing tasks using separate microcircuits that operate in parallel. Such parallel processing is fundamental to brain function[2], including in the vertebrate retina[3,4]. Here, stimulus-response relationships become increasingly specific as the visual signal travels from photoreceptors via bipolar cells (BCs) to retinal ganglion cells (RGCs). Based on this architecture, progressive circuit optimisation for distinct tasks can then take place in different populations of inner retinal neurons. A key question then is: at what stage in the retinal circuit does specialisation for each processing task occur? Optimisation for one task may precede optimisation for others. In teleost fish, for example, substantial investment in spectral coding in the outer retina[5] precedes the extraction of key spatiotemporal features of the inner retina[6].

In larval zebrafish, splitting of "colour" and "brightness" signals begins in the outer retina, where the cone-photoreceptors are modulated by horizontal cells at the first synapse in vision[7]: Red-cones provide an output that signals brightness and is essentially "colour"-invariant, while green-cones provide a primary "colour" output that is brightness-invariant. Further, blue and UV-cones provide secondary "colour" and brightness channels, respectively. Such efficient representation[7–10] of spectral information is beneficial for colour vision, but also poses a new conceptual conflict. For these representations to reach the brain, the signal must pass through the remainder of the retina, where the dense interconnectedness of inner retinal circuits[11–13] alter the original cone signals. However, visual circuits that are not primarily set-up to deal with spectral information are nonetheless forced to work with the heavily pre-processed spectral channels provided by the cones. Despite this conflict, distinct types of BC do represent the spectral inputs from each of the four cone-signals in isolation, alongside a plethora of other BCs that represent diverse cone-mixtures, presumably specialized for other temporal and spatial processing tasks[14,15]. These tasks depend crucially on microcircuits within the inner retina, where amacrine cells (ACs) modify the visual signal by inhibition through both GABA- and glycinergic transmission alongside a variety of neuromodulator functions[13,16–18].

ACs are the most diverse yet least understood class of neurons in the retina[6,19,20]. In mice, transcriptomic analysis revealed 63 molecularly distinct types of ACs[21], thus outnumbering their 15 types of BCs[22] by a factor of more than four. In zebrafish, the number of AC types is not known, however, in view of their >20 anatomically defined BC types[11] it seems unlikely their AC diversity is lower than in mice. At a general level, ACs are thought to shape receptive field structures of BCs and RGCs[13,19], modulating their dynamic range[23,24] and contributing to their diversity[12]. Accordingly, we may expect ACs to contribute to both chromatic and achromatic signalling[25–27]. Yet, beyond a handful of well-studied AC-circuits[24,28–32], mostly in mammals, the specific functions of most AC-types across any species remains unknown.

To test if and how ACs contribute to inner retinal processing by zebrafish BCs, we used *in vivo* two-photon imaging to compare BC responses to a battery of visual stimuli in the presence and pharmacological absence of AC-mediated inhibition. Surprisingly, we find that the population representation of spectral contrast[5,33] (i.e. colour opponency) was approximately unchanged despite profound changes in other aspects of circuit function, such as the gain and kinetics of visual responses, spectral bias and the degree of synchronization between different neurons. However, this was not because opponency in individual BCs was invariant to AC-block. On the contrary: ACs both routinely abolished and generated spectral opponency at the level of individual BCs, but they did so in approximately equal measure, such that the net change across the population of BCs was essentially

zero. To preserve the balance between different chromatic and achromatic channels, ACs act near-exclusively through On-circuits. The notion that ACs are not primarily set up to process spectral information was further supported by a functional survey of ACs themselves: despite being highly diverse – for example in terms of kinetics and polarity - ACs were mostly non-opponent and spectrally resembled linear combinations of UV- and red-cone signals, which in zebrafish are associated with achromatic processing[7]. The only exception to this rule occurred for a small number of weakly colour-opponent On-stratifying ACs, in line with most AC-BC spectral processing being implemented via On-circuits.

We conclude that the parsing of colour information performed in the outer retina is conserved as the visual signal is transmitted to RGCs in the inner retina. The complex interactions within the inner retina that underly other visual processing tasks do not notably alter the population representation of colour information.

RESULTS

Bipolar cell signalling in the presence and absence of inhibition from amacrine cells. To investigate the effects of AC-mediated inhibition on the visual signal transmitted through the inner retina of zebrafish, we combined pharmacology with two-photon (2P) *in vivo* imaging of BC synaptic terminals sparsely and randomly expressing the calcium biosensor SyGCaMP3.5 using established protocols[14,34,35] (Figure 1A-J, Methods). The sparse labelling was essential for observing individual terminals across experimental conditions.

In each experiment, we first scanned a single eye region comprising typically 20-30 individual BC terminals (Figure 1D) and presented a battery of widefield light stimuli testing basic visual processing tasks (Methods): (i) an achromatic ("white") step of light (3 s On, 3 s Off, 100% contrast) testing response polarity and kinetics (Figure 1H); ii) a frequency modulated "chirp" centred at 50% contrast testing frequency response (Figure 1H), (iii) steps of light (2 s On, 2 s Off, 100% contrast) at four different wavelengths ('red': 592 nm; 'green': 487 nm; 'blue': 420 nm; 'UV' 382 nm) testing spectral sensitivity (Figure 1I) and (iv) 'tetrachromatic binary noise' (5 mins, 6.4 Hz, 100% contrast) which allowed us to extract four 'spectral sensitivity kernels' per terminal to probe for spectral opponency (Figure 1J, Methods). This set of stimuli was chosen to facilitate comparison with previous work[7,12,15,36,37], and to test a wide range of achromatic and spectral BC signalling properties within a limited recording time. Next, we injected a cocktail of gabazine, TPMPA, and strychnine into the eye to pharmacologically block $GABA_A$, $GABA_C$ and glycine receptors, respectively[38] (Figure 1B,C, Methods), which represent the major known sources of AC-mediated inhibition in the inner retina[16]. We then imaged the same eye-region a second time (Figure 1F). This strategy allowed us to identify the same terminal in 40-60% of cases (Figure 1D,F, right, Methods). The remainder of non-paired terminals was also captured in both conditions and processed separately. This allowed us to directly compare the effects of AC-block on individual terminals ("paired data"), while also assessing responses across a larger population of all imaged terminals, as appropriate ("all data").

In total, we recorded n = 14 scan-field pairs in an equivalent number of fish, yielding a total of n = 182 paired terminals amongst a total of n = 412 (control) and n = 441 (AC-block) terminals. Because retinal regionalisation[15,37,39] was not a focus of this study, we sampled approximately evenly from all positions in the eye. Moreover, the location of terminals across both datasets covered the entire depth of the inner plexiform layer (IPL) and recovered the notable dip near the centre where BC terminals are less abundant[15,40] (Figure 1E,G), indicating that a representative fraction of all BC-terminals was captured. This approach revealed a range of effects of AC-block on BC functions.

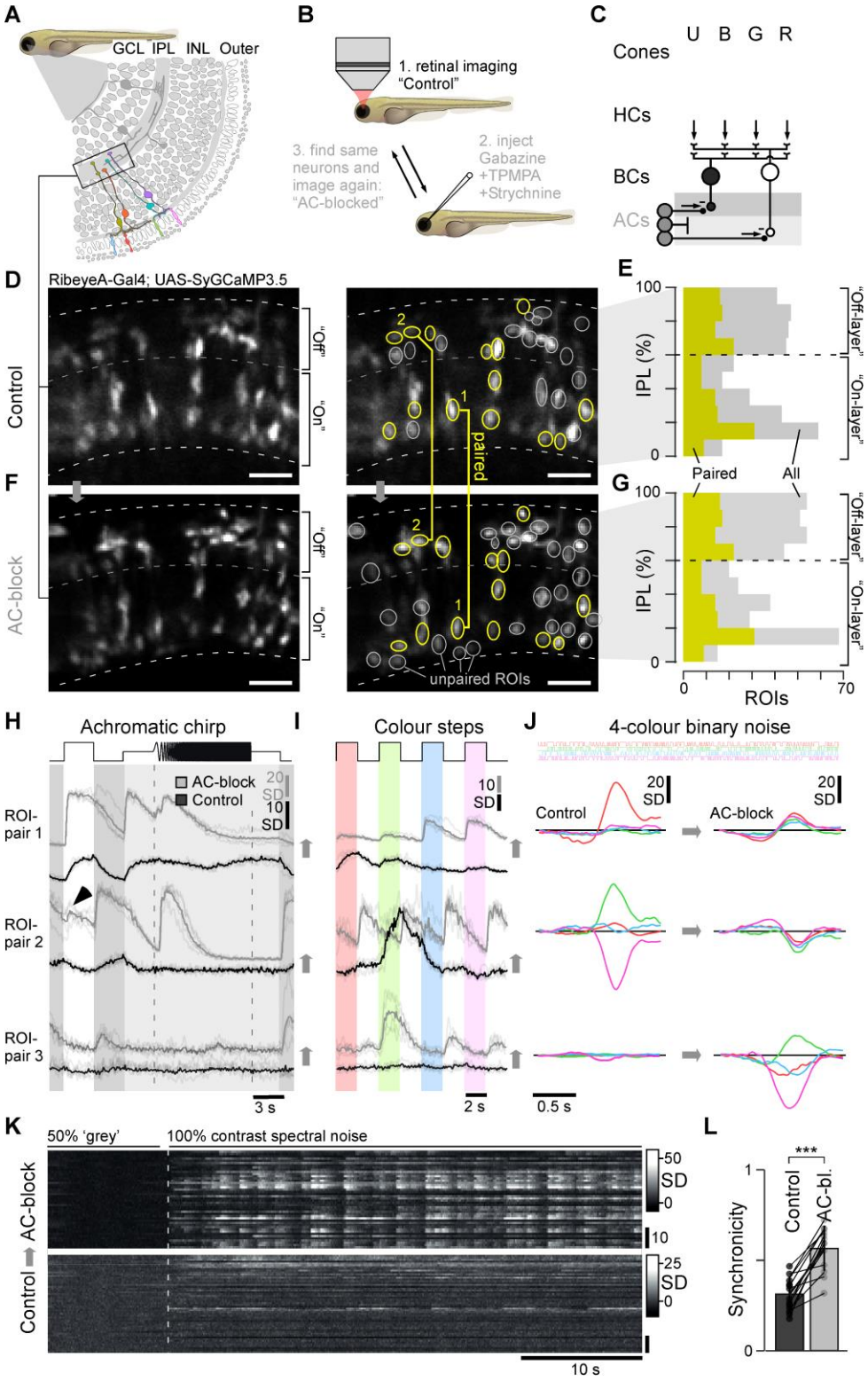

***Figure 1 | Recording bipolar cells before and after amacrine cell block. A**, Schematic cross-section of larval zebrafish retina, with recording region across the inner plexiform layer which houses the synaptic terminals of bipolar cells (BCs) indicated (based on Ref[58]). **B**, Outline of experimental strategy. **C**, Overview of the general circuit logic of the outer (top) and inner retina (bottom): Input is provided by four types of cone-photoreceptors: UV-cones (U, expressing SWS1 opsin), "blue"-cones (B, SWS2), "green"-cones (G, RH2) and "red"-cones (R, LWS1)[5]. Rods are functionally immature in larval zebrafish[59,60]. Cones feed into three types of Horizontal cells (HCs) which, amongst other functions[61], serve to retune the cone output spectra[7,62,63]. This signal is differentially integrated by the dendrites >20 types of BCs[11,14,15,64] and propagated to their axon terminals located in the inner plexiform layer[65]. From here, BCs form synapses with retinal ganglion cells (RGCs, not shown) which form the optic nerve, and with amacrine cells (ACs). ACs in turn provide feedback and/or feedforward inhibition to BCs and RGCs via GABA and/or glycinergic transmission[20]. **D-G**, left, example scan region*

of the inner retina showing sparse syGCaMP3.5 expression in BC synaptic terminals before (D) and again after injection of GABAzine, TPMPA and Strychnine into the eye (F), and the same area with regions of interest (ROIs) superimposed (right); scalebars = 10 µm. ROIs in yellow could be matched across the two experimental conditions and are henceforth considered "paired". The remainder of unpaired terminals was also extracted and processed alongside the paired data ("all data"). The spatial distribution of all terminals processed in this way across n = 14 scan fields is shown with approximate labelling of the traditional "Off" and "On" layers of the IPL. ***H-J****, example responses of three pairs of BC terminals, as indicated in (D,F), to the three light stimuli tested: an achromatic chirp stimulus (H), four spectrally distinct steps of light from dark (red, green, blue, UV, as indicated, Methods) (I) and a spectral noise stimulus used to establish linear filters (kernels) at the same four wavelengths (J). In each case, the control data (black) is shown alongside the corresponding AC-block data (grey). The top two pairs correspond to the ones highlighted in (D-G), while pair 3 is taken from a different scan.* ***K,L****, comparison of population synchronicity during spectral noise stimulation (J). Heatmaps show the first 60 s of the z-normalised responses of all terminals in control (bottom) and AC-block condition (top) taken from the same scan-field. Population synchronicity (L) was computed as in Ref[42]. Wilcoxon Signed-Rank test: $p = 2.4*10^{-4}$. The black arrowhead in (H) highlights an unmasked small On-response.*

Changes in response amplitude. Blocking inhibition increased the amplitude of responses to achromatic steps of light without changing the dominant response polarity (Figure 1H), consistent with role of ACs in controlling the gain of the synaptic output from BCs[41]. For instance, ROI-pair 1 consistently exhibited On-responses, but with a notably increased amplitude and altered time course following AC-block (grey) compared to control conditions (black). ROI-pairs 2 and 3 exhibited Off-responses both during control conditions and following AC-block, again with increased amplitude and altered time-course. In the case of ROI-pair 2, AC-block also unmasked an additional low-amplitude On-response.

Changes in colour coding. ACs served to spectrally sharpen or retune 'intrinsically broad' responses in individual BCs. For instance, in ROI-pair 1, responses to colour steps (Figure 1I) were red-biased during control condition but responded to all four wavelengths after blocking inhibition, and this spectral broadening was also observed at the level of the kernels (Figure 1J). It appears that in this case ACs were masking an intrinsic short-wavelength response to set-up a long-wavelength biased BC. The effects on ROI-pairs 2 and 3 were opposite: ROI-pair 2 exhibited a green-UV colour-opponent response during control conditions, which was abolished following AC-block, while vice versa ROI-pair 3 exhibited weak non-opponent response during control conditions but green-UV opponency upon AC-block. Accordingly, in ROI-pair 2, ACs were responsible for setting up BC-opponency, while in ROI-pair 3 ACs masked an intrinsic form of BC-opponency.

Changes in signal correlations. In mice, inhibitory networks in the inner retina decorrelate signals transmitted through BCs which reduces redundancy across the population[12]. We therefore compared activity across the population of BC synapses in response to stimulation with spectral noise (Figure 1K,L, cf. Figure 1J) before and after AC-block at a population level. Here, our reasoning was that the removal of inhibitory neurotransmission should not only lead to a disinhibition of BCs (leading, for example, to larger responses), but also to an increased synchrony across the population. Using a normalized synchrony measure, $\chi(N)$[42], this is indeed what we observed (Figure 1K,L). Accordingly, like in mice[12], the removal of inhibition served to decorrelate BC responses also in zebrafish.

In addition to the AC-block dataset, we also recorded an equivalent but independent sham control dataset (n= 6 scans, n = 144 paired terminals amongst a total of $n_{Control}$ = 398, n_{sham} = 378 terminals), where we replaced the drug cocktail used to block ACs with an equivalent volume non-pharmacologically active vehicle. Sham injections had no significant effect on the functions we analysed (Supplemental Figure S1A-H, Methods). Finally, we also evaluated the effect of 'AC-block' on outer retinal function, using the known horizontal cell-mediated red-opponency in green-cones [7] as the test case. This confirmed that green cones' red-opponent responses persisted in the presence of the drug-cocktail (Supplemental Figure S1I-K).

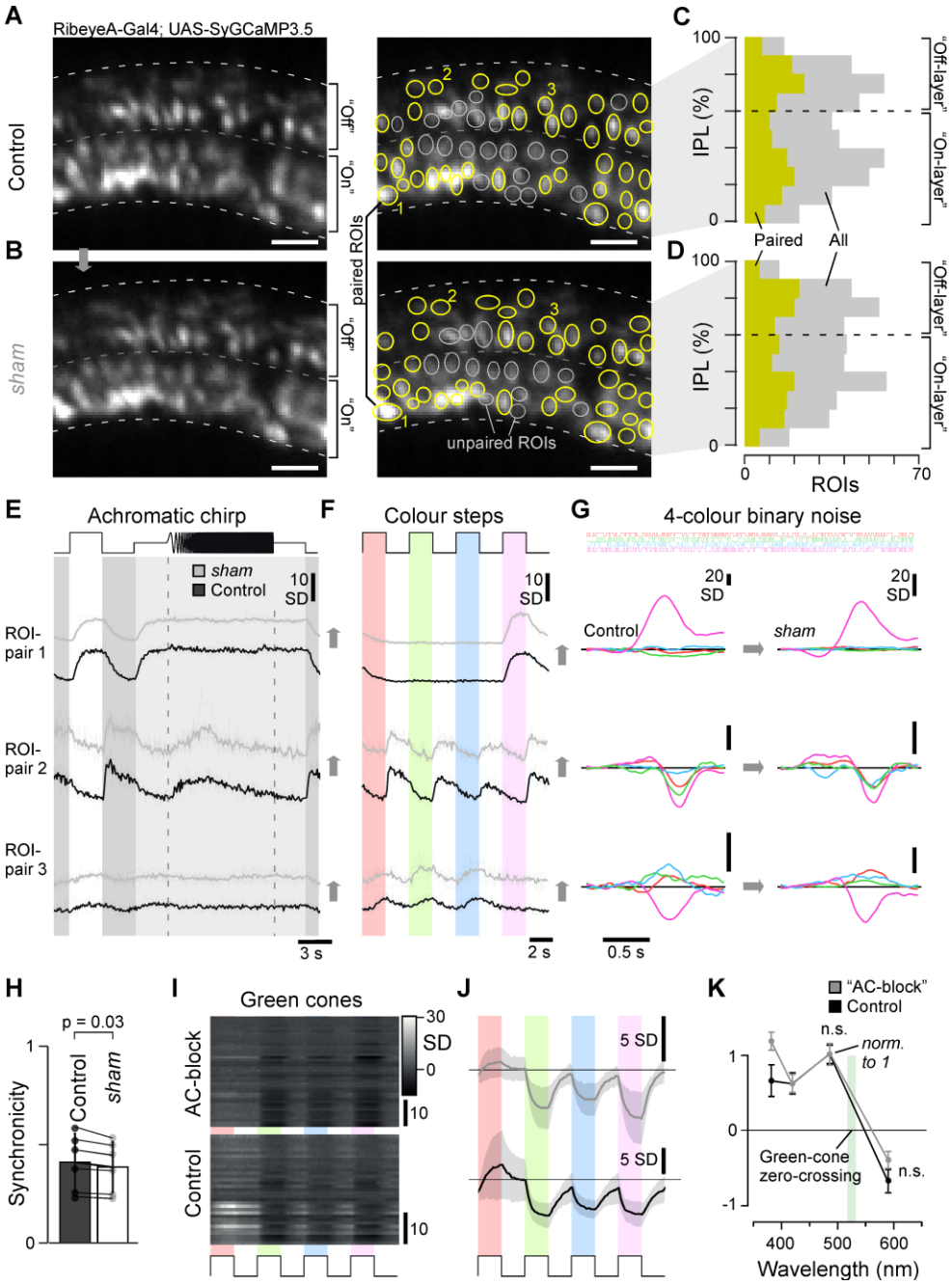

***Supplemental Figure S1 – related to Figure 1**. **A-G**, as Figure 1D-J, but for an example sham-injection dataset. **H**, as Figure 1L, but for sham-injection datasets. Wilcoxon Signed-Rank test: p = 0.03. **I-K**, No effect of drug-cocktail injection as in Figure 1 on spectral opponency in green-cones. Heatmaps (I) of SyGCaMP6f responses in green-cone terminals to the four steps of light as Figure 1I (based on previously established protocols before (bottom) and after drug injection (top), the same data summarised with mean±1SD shading (J) and extracted response amplitudes plotted against stimulus wavelength (K). The green shading indicates the spectral position of the green-cones' zero-crossing from Ref[7]. Wilcoxon rank sum test, p = 0.87, 0.07 for red and green responses, respectively. Note that green-cone responses continue to invert between mid- (green) and long-wavelength stimulation (red) following AC-block, indicating that cone-opponency is not affected by this manipulation.*

Below we expand these specific examples to a broader evaluation of the effects of AC-block on achromatic BC-functions and link these to different possible cone-photoreceptor systems using the spectral steps. We then evaluate the dominant AC-mediated effects on population coding of colour using the kernels.

ACs attenuate BC gain and kinetics without affecting response polarity. To evaluate the effects of AC-block on the encoding of the 'white' step of light, we fitted trial-averaged achromatic step-responses using a linear kinetic model following a similar approach used in recent work[14]. Briefly, the model used four kinetic templates to capture the dominant response waveforms across our datasets: Light-transient, Light-sustained, Dark-transient, and Dark-sustained (Figure 2A-E, Methods). This allowed simplifying the often-complex interplay of different response-components into four corresponding weights. For example, the BC shown in Figure 2A exhibited a relatively slow On-response in the control condition that was readily captured by a positively weighted Light-sustained component alone (Figure 2C, bottom). However, the same BC's response following AC-block was kinetically more complex. Capturing this compound waveform required the additional use of a large light-transient component alongside the continued presence of the light-sustained component (Figure 2C, top). Moreover, the response decay following the light step was marginally faster than in the control condition and required the additional use of low amplitude negative dark-component weights. Accordingly, in this case the kinetic model predicted that the main effect of AC-block was the unmasking of a light-transient response, potentially with addition of a smaller suppressive dark-response. The same approach served to fit all achromatic step-responses across conditions. For example, the Off-responses shown in Figure 2D were well captured by the combination of a negative light-sustained component, alongside the unmasking of a positive dark-transient component following AC-block. Similarly, the model also captured well another BC's On-Off response that was unmasked following AC-block (Figure 2E). Across all datasets, the model consistently captured >95% of the variance across the respective response means (Supplemental Figure S2A,B, Methods). The extracted component weights were used as the basis for all further analysis of step responses.

First, we automatically sorted all responses by polarity (Methods), applying a minimum component weight threshold of 3 SDs to constitute a response (Figure 2F-J). Based on this criterion, the n = 412 control BCs (full dataset) were sorted into n = 266 (64%) non-responsive BCs, n = 76 On BCs (18%) and n = 70 Off BCs (17%, Figure 2F, bottom, cf. Figure 2G,H). Under control conditions, no BC was classed as On-Off. Correspondingly, the n = 442 AC-block BCs were sorted into n = 59 non-responsive BCs (13%), n = 240 On BCs (54%), n = 122 Off BCs (28%), and n = 20 On-Off BCs (5%, Figure 2F, top, cf. Figure 2G,H). No major changes were observed in the sham-injection dataset (Supplemental Figure 2C). Accordingly, at a population level, the removal of inhibitory inputs from ACs revealed previously unresponsive BCs, a major rebalancing of On- versus Off-signals and, unexpectedly, unmasked the presence of a small fraction of On-Off BCs. Despite this rebalancing, the anatomical distributions of different polarity BCs within the IPL were largely conserved following AC-block: Under both conditions, On- and Off-responding BCs dominated the lower- and upper part of the inner retina, respectively (Figure 2G). However, in all cases at least a small fraction of On- and Off-terminals was found outside these "traditional Off-" and "On-layers"[43], respectively (see also Refs[14,15]). Interestingly, On-Off cells were predominately unmasked in the "Off-layer", suggesting a closer relationship with Off- rather than On- BCs.

Next, we used the "paired" subset of BCs (n = 182) to evaluate how this polarity-shift emerged at the level of individual terminals (Figure 2I). This revealed that AC-block inverted the polarity of individual terminals in only n = 4 / 182 cases (2%). Instead, most terminals that exhibited light-responses during control conditions continued to exhibit the same polarity following AC-block (n_{On} = 43/44, n_{Off} = 19/29). The bulk of observed changes (cf. Figure 2F-H) rather stemmed from the unmasking of light responses in previously unresponsive terminals (n = 101/182, 55%). Most unmasked terminals were On (69) rather than Off (23) or OnOff (7). Accordingly, a key role of ACs in the zebrafish retina appears to be in modulating the gain of BCs' 'photoreceptor-inherited' light responses, without routinely inverting their polarity. This modulation could be very powerful, masking BCs'

photoreceptor-inherited light responses to the widefield achromatic stimulus altogether in more than half of all cases.

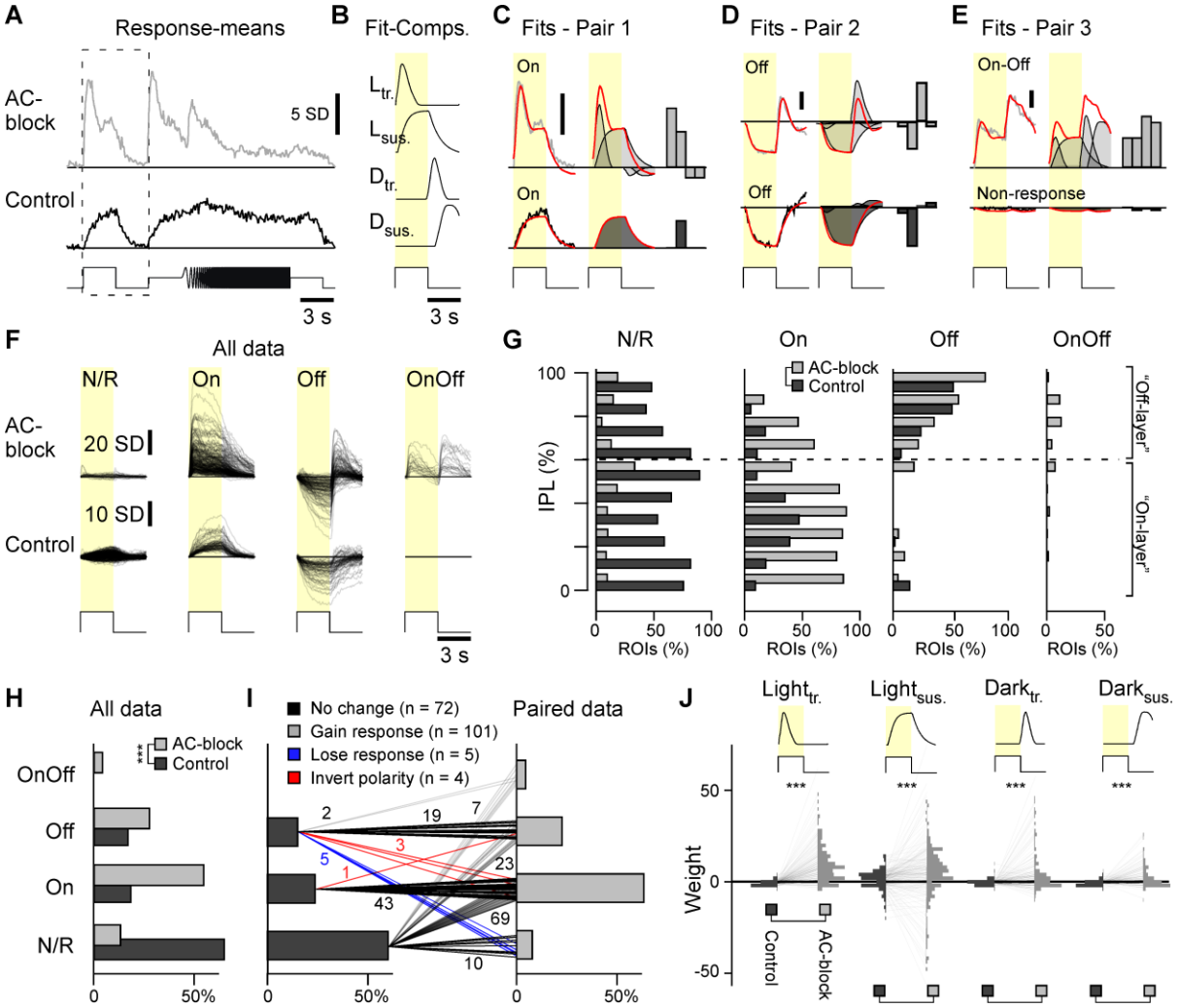

***Figure 2 – Major effects of AC-block on achromatic BC-functions. A-E**, Example responses to the 'white' chirp stimulus (cf. Figure 1H) and template-fitting approach (Methods). One pair of example BC terminals is shown in (A), with the stimuli illustrated under the response traces. Four kinetic templates (B) are used for fitting the response to 'white' step stimuli, three examples of fitting results are shown in C-E. In each graph, left panel, the black/grey traces represent single BCs' average responses for control/drug condition, with fits in red; middle panel, the fits plotted with the four weighed templates, with corresponding weights, left to right: Light-transient, Light-sustained, Dark-transient, and Dark-sustained respectively. **F-H**, All BCs automatically sorted by polarity ($n_{control}$ = 412, $n_{AC\text{-}block}$ = 441). Traces from all BCs shown superimposed (F), their respective IPL positions shown in (G), and group percentages shown in (H), Chi-squared test, $p = 5.51*10^{-54}$. **I**, as (H), but for the subset of paired BCs (n=182 pairs), showing pairwise allocations in control (left) and AC-block conditions (right). Lines represent the pairs, with numbers of BCs indicated. Chi-square test, $p = 4.59*10^{-25}$. **J**, Pairwise weight distributions for the four kinetic components (B) in control (left) and AC-block condition (right), as indicated.*

To evaluate effects on BCs' gain and kinetics following AC-block, we next analysed the pair-wise change in each of the four kinetic component weights (Figure 2J). This revealed that most changes occurred amongst light- rather than dark-components, and the weights of transient components tended to change more strongly compared to the weights of sustained components (Supplemental Figure 2D, cf. Figure 2C,D,F). Moreover, most changes were positive in sign – that is, accentuating the stimulus-driven rise in calcium signals. The only systematic exception to this rule occurred amongst a subset of light-sustained components, which showed an accentuated decrease instead.

Overall, our results show how ACs fundamentally shape essential achromatic circuit functions such as the gain and kinetics of BCs. We next asked if and how ACs shape the encoding of BCs' spectral information.

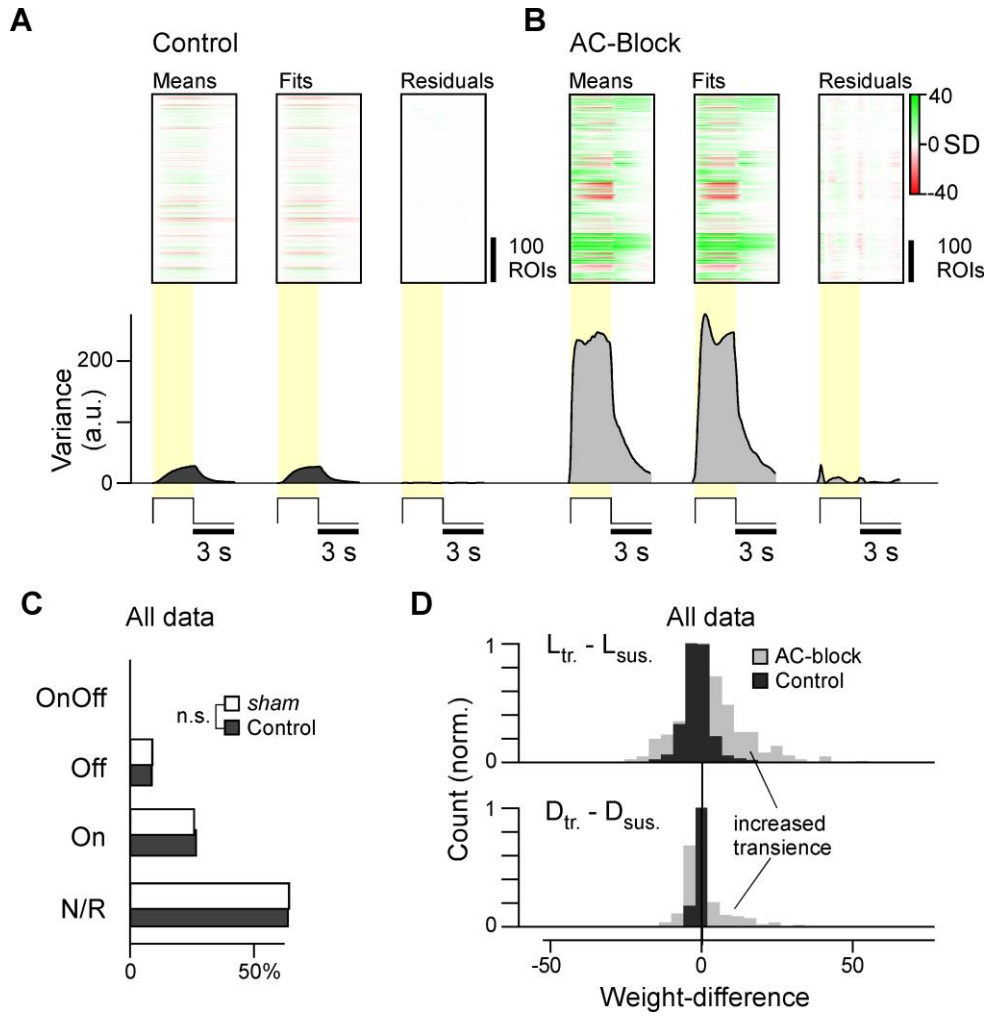

***Figure S2 – related to Figure 2. A,B**, Summary of fits for all achromatic step responses (cf. Figure 2A-E). Heatmaps show the population data in control (A) and AC-block condition (B). In each case, the first column represents all BCs' trial-averaged achromatic step responses, followed by the corresponding fits and the residuals. In each case, the variance across a heatmap's y-dimension, indicative of the overall signal in each dataset, is shown below (see also Ref[14]). **C**, as Figure 2H, but for sham-injection dataset. **D**, Paired weight differences between transient and sustained components in control and AC-block conditions as indicated (light and dark-components in top and bottom, respectively). Wilcoxon rank sum test, $p = 1.41*10^{-11}$ for $L_{tr.} - L_{sus.}$, $p = 0.08$ for $D_{tr.} - D_{sus.}$.*

ACs shape spectral BC-processing but preserve colour opponency. To distinguish changes in wavelength from changes in intensity, circuits for colour vision spectrally contrast signals of different photoreceptor systems[5,33]. The resultant "colour opponent" neurons might be considered the fundamental 'currency' of colour vision. Accordingly, we next assessed the impact of AC-block on the representation of colour opponency amongst BCs.

In zebrafish, BCs represent three types of spectral opponency (Supplemental Figure 3A, see also Supplemental Figure 3B-E): "Long-" ("red-green"), "mid-" ("orange-blue") and "short-" ("yellow-UV"), with spectral zero crossings at ~523, ~483 and ~450 nm, respectively[14,15]. Of these, long- and mid-wavelength opponency is already encoded at the level of green- and blue-cones, respectively[7]. Accordingly, ACs are not categorically required to set-up these types of opponency in BCs. In contrast, short-wavelength opponency is only weakly represented in UV-cones[7], but dominant amongst BCs[14]. Therefore, the expectation is that this short-wavelength type of opponency in BCs requires the presence of ACs.

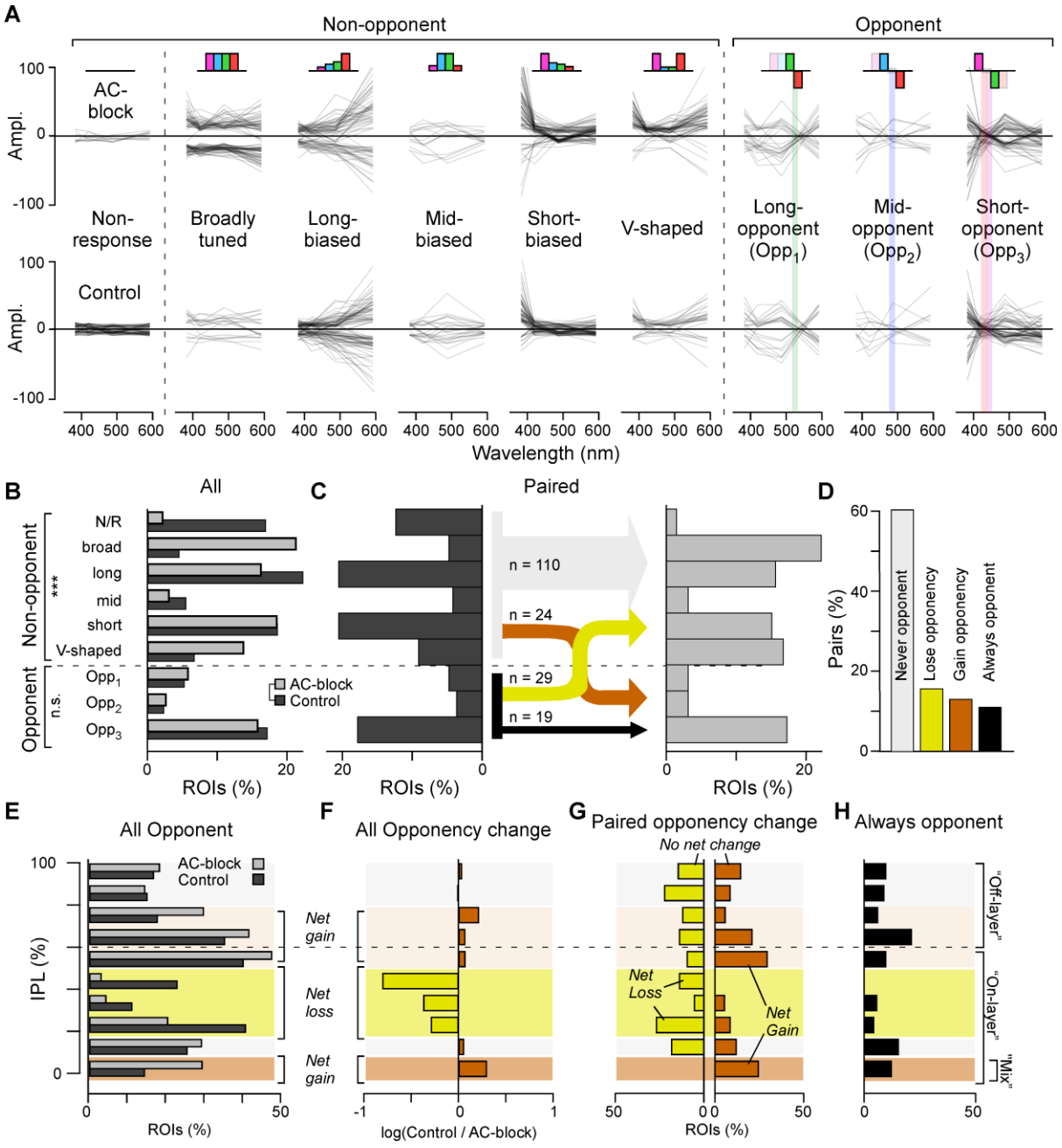

Figure 3 – Modulation of spectral processing. A-F, *All BCs' spectral tuning functions (based on the kernels, cf. Figure 1J) under control (bottom) and AC-block condition (top) sorted into nine groups as indicated (Methods). The shaded bars in the three opponent groups (right) indicate their corresponding spectral zero crossings (based on Refs[7,14] – cf. Supplemental Figure 3A).* ***B-D,*** *Percentages of ROIs in each spectral group for all data (B) and paired data (C). In 'all data', black and grey bars represent control and AC-block conditions, respectively. For simplicity, the individual 9-fold category correspondences in the paired data are summarised into non-opponent and opponent groups, leading to four forms of correspondences between control (left) and AC-block condition (right): always non-opponent (grey); always opponent (black); Lose opponency upon AC-block (yellow), gain opponency upon AC-block (orange/brown). Percentages of these four groups are further summarised in (D). Chi-squared tests: all data (B), $p = 2.44*10^{-22}$ (non-opponent group) and p = 0.81 (opponent group); paired data (C), $p = 3.9*10^{-8}$ (non-opponent group) and p = 0.81 (opponent group).* ***E-H****, Data from (A-D) summarised by IPL position with (E,F) and (G,H) summarising all- and paired-data, respectively. IPL distributions of opponent BCs under control and AC-block condition (E) and their relative change (F), with IPL regions with net loss (yellow) and gain of opponency (orange/brown) highlighted. Based on paired data, IPL distribution of BCs that lose (G, left, yellow) and gain opponency (G, right, orange) and those that are always opponent (H). Shadings behind E-H indicate approximate regions of the IPL that tended to exhibit a net loss (yellow) or gain (orange/brown) of opponency following AC-block, or where opponency was approximately balanced (grey).*

Surprisingly, neither of the above expectations were experimentally confirmed. Instead, and despite profound impacts of AC-block on the representation of colour opponency at the level of most individual BCs, the population representation of colour opponency amongst BCs was essentially unchanged following AC-block.

To reach this conclusion, we first automatically sorted all BC-responses in control condition, and again following AC-block, into one of nine spectral groups, which included non-responders, five non-opponent groups (broad, long-, mid-, short-wavelength biased, V-shaped), and three opponent groups (long-, mid- and short-wavelength opponent) (Methods). This revealed that the overall representation of all nine groups remained approximately constant, in the sense that under either condition, a substantial fraction of BC-responses fell into each spectral group (Figure 3A). Nevertheless, in agreement with the results from the achromatic step responses (Figures 2), the relative abundances amongst non-opponent groups did change. Most notable was a pronounced decrease in the abundance of non-responders (17.0% → 2.3%) alongside a marked increase in the proportion of broadly tuned (4.6%→ 21.3%) and V-shaped BCs (6.8% → 13.8%). These changes were accompanied by more minor reductions in the proportions of long- (22.3% → 16.3%) and mid-wavelength biased BCs (5.6% → 3.2%). However, strikingly, the relative abundances of all three opponent groups (long: 5.3% → 5.9%; mid: 2.4% → 2.7%; short: 15.8% → 17.2%), alongside those of short-wavelength biased BCs (18.7% → 18.6%), remained largely unchanged. Accordingly, at a population level, and despite the major rebalancing of response amplitudes and kinetics (Figures 1,2), the removal of AC influences had negligible effects on population coding of colour opponency through BCs (Figure 3A,B).

However, remarkably, analysis of the paired-dataset (Figure 3C) revealed that this was not because colour opponency in individual BCs was unaffected by AC-block. On the contrary: More than half of all BCs that exhibited opponency under control conditions lost opponency following AC-block (n = 29 of 49, 59.2%). However, at the same time, an almost equal number of previously non-opponent BCs replenished the population of opponent BCs (n = 24). This "switching" of opponent BCs between conditions affected all three opponent groups: of the n = 8, 7 and 33 long-, mid- and short-wavelength opponent BCs recorded during control conditions, respectively, only n = 2, 2 and 15 (25%, 29%, 45%) BCs, respectively, maintained their specific opponency following AC-block. Except for a single BC that switched from long- to short-wavelength opponency, all remaining opponent BCs lost their opponency altogether following AC-block (Figure 3C,D). Examples of diverse opponency-relationships between control and AC-block conditions are presented in Figure 4.

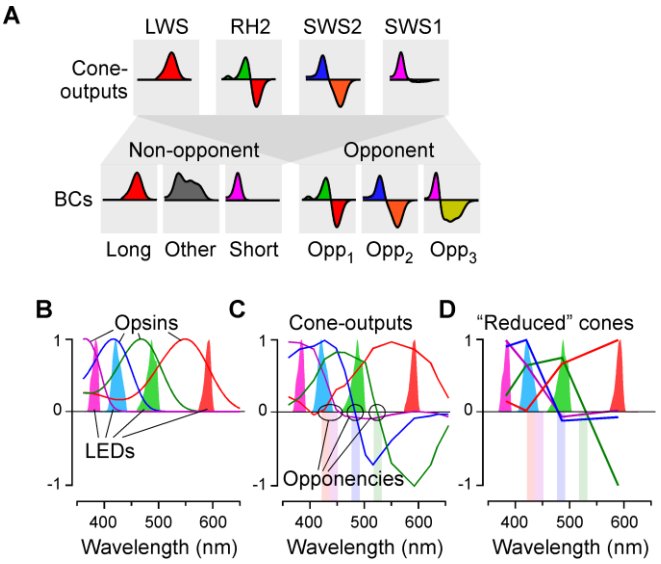

***Figure S3 – related to Figure 3. A**, Illustration of how cone input could build the different spectral response types in BCs. Insets indicate approximate spectral tuning functions (amplitude y versus wavelength x). The upper row shows the four cones[7], bottom rows shows BCs[14,15], divided into non-opponent group and opponent group. **B-D,** Summary of known spectral tuning functions of cones and their opponencies (based on Ref[7]). In each panel, the four LEDs used in the present study are shown as solid curves (Methods). Superimposed are the spectral tuning functions of the cone opsins (B), their in vivo spectral tuning functions with zero crossings indicated (C), and the cones' spectrally "reduced" in vivo tunings functions as probes with the four LEDs.*

Unexpectedly, therefore, ACs contributed to building all three types of colour opponent responses found amongst BCs; however, at the same time, they also masked pre-existing opponency in other BCs in approximately equal measure such that the net change was essentially zero.

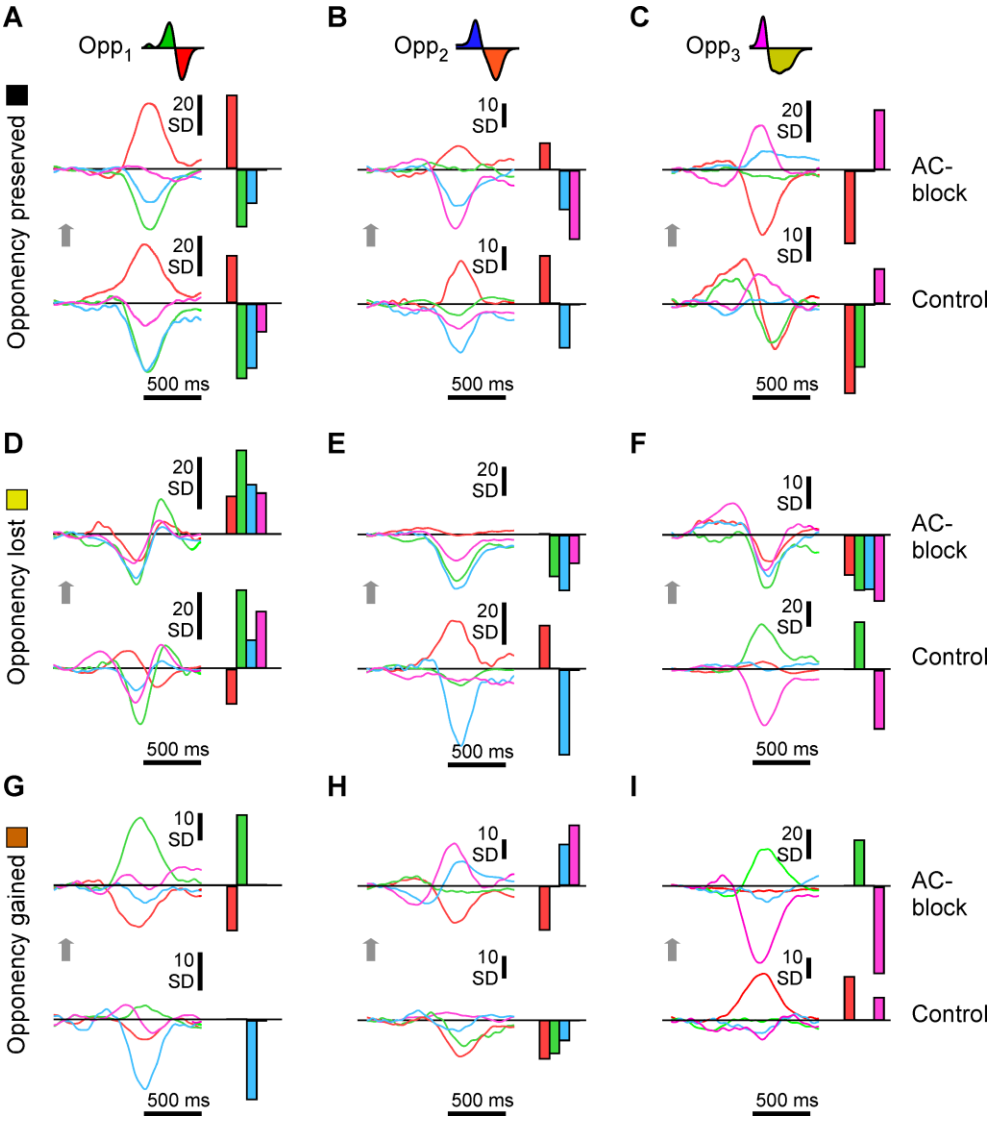

***Figure 4 – Preservation, loss and gain of BC opponency following AC-block. A-I**, Selected example BCs (paired data) that either preserved (A-C), lost (D-F) or gained (G-I) spectral opponency following pharmacological removal of inner retinal inhibition. Examples from all three types of opponencies are presented: red:green (Opp_1, A, D, G), red/(green):blue (Opp_2, B, E, H), (red)/green:UV (Opp_3, C, F, I). Shown in each case are the four spectral kernels (left) and their automatically extracted response amplitudes (right, Methods).*

Colour opponent BC-circuits occur in different parts of the inner retina in the presence and absence of ACs. Even though across the population of recorded BCs, the relative abundances of the three opponent groups remained approximately unaffected by AC-block, this was not the case with regards to their distribution across the IPL. Instead, blocking ACs reduced the abundance of opponent BCs towards the IPL centre but increased their abundance in the most GCL-adjacent strata as well as around the lower Off-layer (Figure 3E,F for all data, Figure 3G,H for paired data). The spatial pattern of this redistribution is reminiscent of the native distribution of On- versus Off-responses in larval zebrafish (which includes the presence of 'ectopic' Off-terminals beneath the traditional On-layer, Figure 2G, see also Refs[14,15]). It thus appears that upon AC-block, BC-opponency tends to be lost where native On-circuits predominate but gained where native Off-circuits predominate.

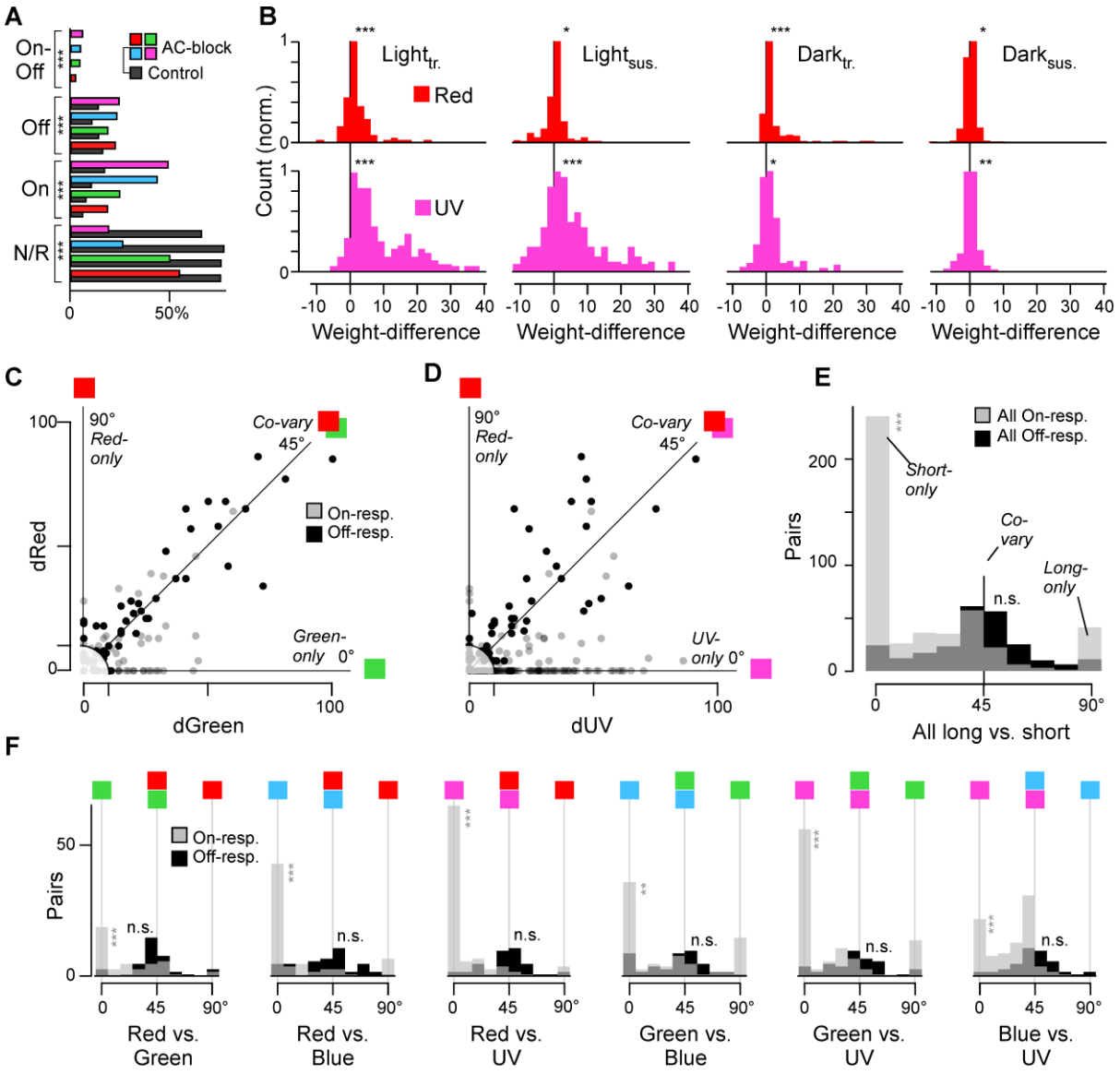

Figure 5 – Selective spectral modulation of the On-pathway. A, *redistribution of response polarities following AC-block (cf. Figure 2H) based on "colour" step responses (cf. Figure 1I). As for "white" steps, each "colour" step response was analysed independently and sorted into four polarity groups (On-Off, Off, On, N/R). Chi-squared tests, p = 3.62*10^{-10} (red), p = 7.74*10^{-16} (green), p = 8.79*10^{-49} (blue), p = 2.87*10^{-42} (UV).* ***B,*** *weight difference of paired red (top row) and UV (bottom row) step responses. From left: Light-transient, Light-sustained, Dark-transient, and Dark-sustained. Wilcoxon Signed-Rank test, for red: p = 1.90*10^{-5} (Light-transient), p = 0.047 (Light-sustained), p = 3.43*10^{-11} (Dark-transient), p = 0.026 (Dark-sustained); for UV, p = 8.5*10^{-24} (Light-transient), p = 5.3*10^{-5} (Light-sustained), p = 0.014 (Dark-transient), p = 0.0012 (Dark-sustained).* ***C-F****, co-variation of absolute response amplitudes changes (in SD) after AC-blockage, compared across different pairs of wavelengths (paired data). (C,D) shows individual scatterplots for red versus green (C) and red versus UV (D). On- and Off-responses plotted separately, as indicated. Angular histograms (E,F) were computed from these scatterplots. In each case, 45˚ indicates co-variation, while peaks around 0˚ and 90˚ indicate that one of the two compared wavelength responses changes independently of the other. Datapoints with an Euclidean distance <10 from the origin were excluded from further analysis (shaded area in C and D). (F) shows the individual comparisons (e.g. the first histogram pair corresponds to the scatterplot shown in (C)), while (E) shows the sum of all six histograms from (F). Note Off-responses tended to co-vary (peak at 45˚), while On-responses exhibited a more diverse distribution, which included peaks are 0˚, 45˚ and 90˚. Wilcoxon Signed-Rank test for each colour combination, tests were performed between On- or Off-angular distributions and 45°: All On (E): p = 1.5*10^{-36}, All Off (E): p = 0.32; Individual On (F): p = 7.9*10^{-5} (red vs. green), p = 1.7*10^{-7} (red vs. blue), p = 3.4*10^{-14} (red vs. UV), p = 0.0048 (green vs. blue), p = 6.8*10^{-8} (green vs. UV), p = 6.1*10^{-9} (blue vs. UV); Off: p = 0.38 (red vs. green), p = 0.97 (red vs. blue), p = 0.24 (red vs. UV), p = 0.56 (green vs. blue), p = 0.89 (green vs. UV), p = 0.30 (blue vs. UV).*

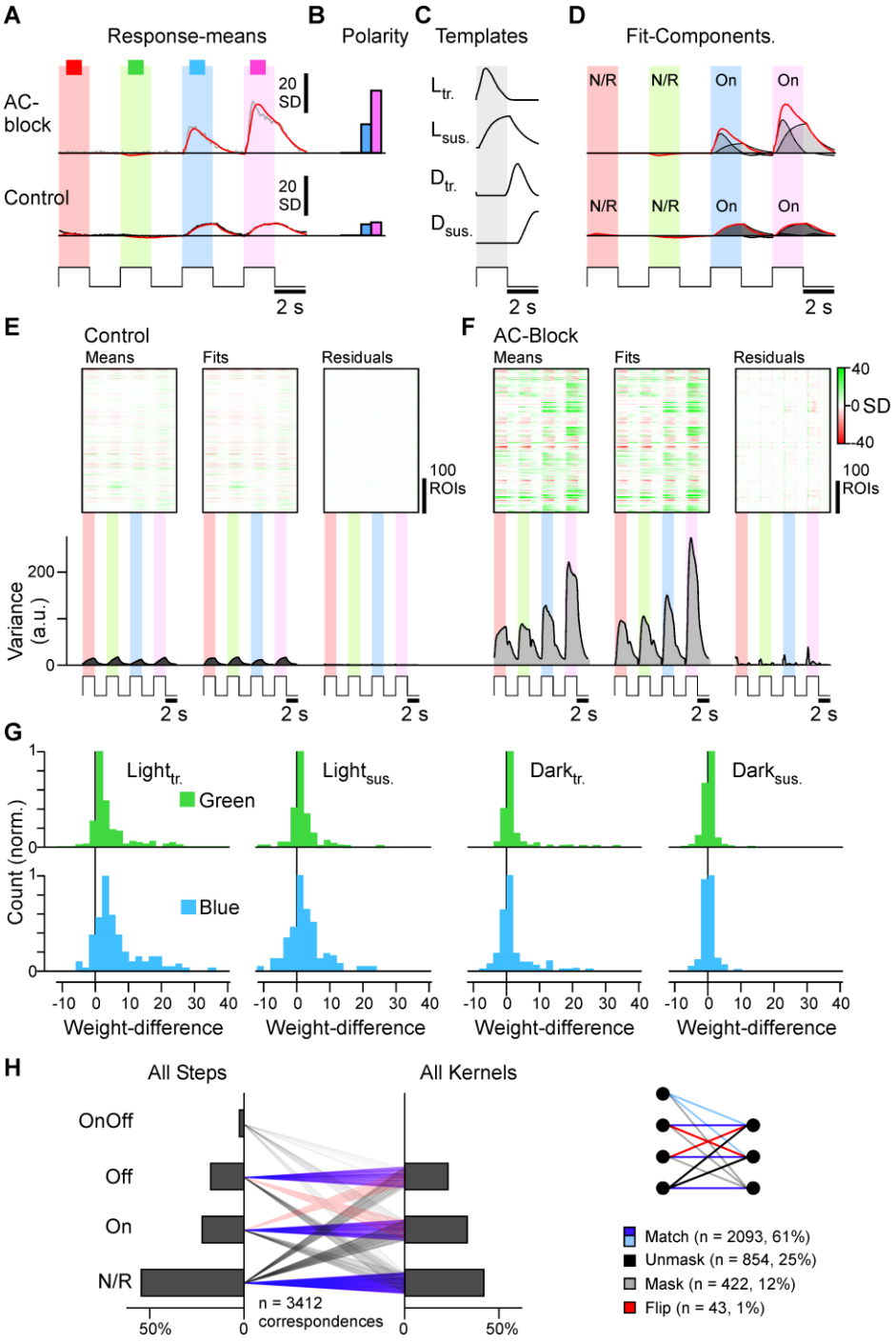

Figure S4 – related to Figure 5. A-D, *template fitting approach for the "colour" step stimulus (cf. Figure 1I, Figure 2A-D). One example pair is shown in (A), with fits (red) plotted superimposed on the trial-averaged colour step responses. Note that for simplicity, the four weights corresponding to each colour-fit are collapsed into a single number (B, Methods). Templates used (C) are truncated versions of those used for fitting white steps (colour steps were 2 s On 2 s Off, while white steps were 3 s On 3 s Off). The full fit result for this example cell is shown in (D).* ***E,F,*** *(as Supplemental Figure 2A,B), evaluation of fit results for the colour steps.* ***G,*** *as Figure 5B, here shown for green and blue. Wilcoxon Signed-Rank tests, green: p = 3.44*10^{-15} (Light-transient), p = 0.15 (Light-sustained), p = 3.64*10^{-6} (Dark-transient), p = 0.062 (Dark-sustained); for blue, p = 1.4*10^{-23} (Light-transient), p = 0.050(Light-sustained), p = 0.0024 (Dark-transient), p = 0.0094 (Dark-sustained).* ***H****, pairwise comparison of individual BC polarities computed from the "colour" steps (left) and kernels (right). For this analysis, each BC contributes eight polarity-values: four for the steps, and four for the kernels. Control and drug data are pooled. Correspondingly, there 412 (control) plus 441 (AC-block) times four correspondences shown (i.e. n = 3,412). Across these, the allocated polarities exhibited a direct polarity match in n = 2,093 cases (61%, purple, 'match'). In contrast, only n = 43 cases exhibited a polarity inversion (1%, red, 'flip'). The remainder of cases occurred when either the steps (n = 854, 25%, 'unmask') or the kernels (n = 422, 12%, 'mask') yielded at non-response despite the respective other measure yielding a response. For further detail, see Methods.*

ACs modulate BC-spectral processing via the On-channel. Based on the anatomical link between the representation of opponency and polarity within the inner retina (Figure 3E,F, cf. Figure 2F-J) we next wondered if generally, spectral processing in On- and Off-circuits was differentially affected by AC-block. For this, we used the "colour-step" stimulus (Figure 1I) and as before (Figure 2A-E) fitted a BC's overall response with a weighted sum of four kinetic "building-blocks" (Supplemental Figure 4A-F Methods; for a comparison of step responses and kernels see Supplemental Figure 4H and Methods). We then analysed each spectral step to again assess the redistribution of response polarities across wavelengths (Figure 5A cf. Figure 2H). This highlighted two main wavelength-dependent effects of AC-mediated inhibition in BC: one, wavelength-specific changes tended to be increasingly pronounced for shorter wavelengths, and two, they mostly occurred in the On-channel.

Under control conditions, the percentages of unresponsive BCs were similar across wavelengths (76%, 76%, 77%, 66% for red, green, blue, UV, respectively); however, following AC-block this ratio fell to 55%, 50%, 27% and 19%, respectively (Figure 5A), indicating that the disinhibition of BC signals following AC-block was most pronounced for UV, followed by blue, then green, and finally red. This short wavelength-bias was essentially restricted to the On-channel, while the Off-channel was boosted in an approximately wavelength-independent manner. The short-wavelength On-bias could also be observed when comparing the changes amongst the four kinetic components (Figure 5B, cf. Figure 2J, Supplemental Figure 4G).

We next used the paired dataset to assess the degree of response co-variation across wavelengths following AC-block (Figure 5C-F). We reasoned any achromatic effects of ACs on BCs should lead to a high degree of covariation across wavelengths, while any spectral 'retuning' of BCs should manifest in some wavelength-responses being affected more than others. The results from this analysis cemented the idea that essentially all spectral modulation of BCs by ACs occurred via the On-channel.

Figure 5C shows On- and Off-amplitude changes in response to the red step of light plotted against the corresponding amplitude changes in response to the green step of light. In this case, most Off-points fell near the equivalence line (45˚), indicating that red- and green-Off response-changes tended to co-vary. Similarly, many On-points fell on the equivalence line; however, in this case, a second population of points fell on or near the 0˚ line. This latter population indicated that in some BCs, response amplitudes changed in green without simultaneously changing in red. Only few points fell on the 90˚ line, indicating a notable absence of On-responses that were modulated in red without also being modulated in green.

To summarise this behaviour, we computed the corresponding angular histogram (Figure 5F, first entry), which showed a single peak around 45˚ for Off-responses indicating mostly co-variation, but two main peaks for On-responses: one at 45˚, and another at 0˚. This general pattern was stable for all possible colour combinations (Figure 5D-F). In the On-channel, but not in the Off, shorter wavelength responses were consistently modulated more strongly than long wavelength responses. The only spectral combinations that exhibited any appreciable degree of long-wavelength isolation were green versus blue and green versus UV (peak at 90˚ in 4th and 5th entries in Figure 5F), indicating a putative 'special' role of AC-inputs for modulating green-On circuits.

Taken together, our data overwhelmingly support the idea that ACs modulate the gain of short-wavelength responses predominately, and notably point to the On- rather than the Off-channel for shaping spectral tuning amongst BCs. This spectral On-channel dominance can also be appreciated in example cases of both non-opponent (Figure 6A-D) and opponent BCs (Figure 6E-H).

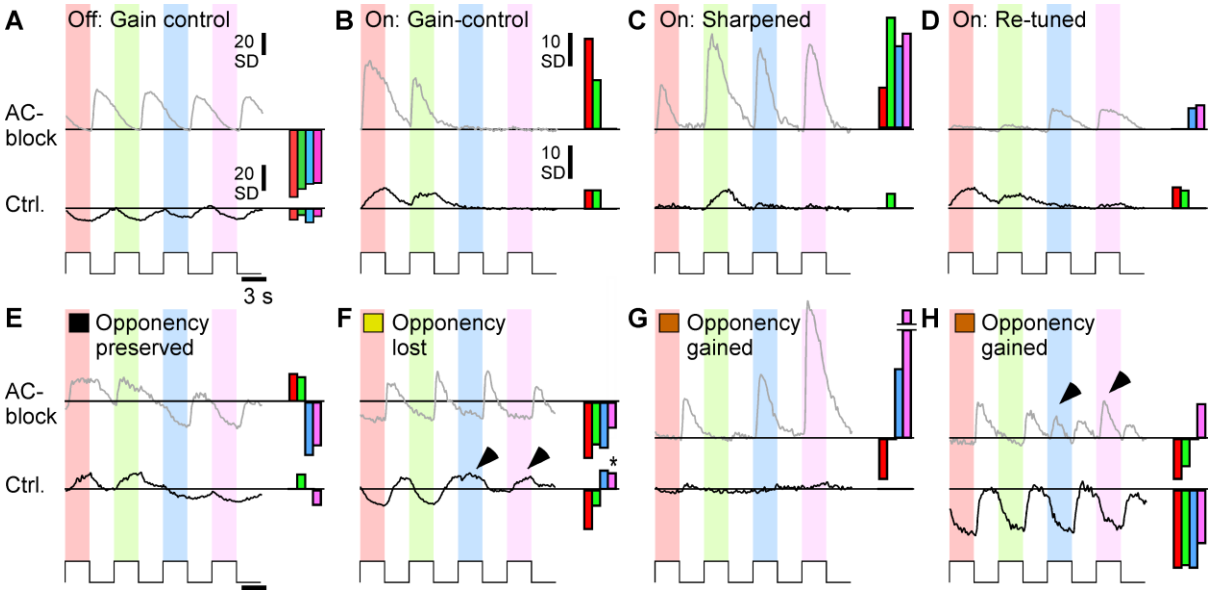

Figure 6 | Spectral re-tuning mainly uses the On-channel. A-H, *Selected example BC "colour" step responses (trial averages) during control condition (bottom) and following AC-block (top, paired data), illustrating a range of 'typical' results. Generally, changes in Off-responses tended to be similar across all tested wavelengths (e.g.: A). In contrast, changes in On-responses tended to be more spectrally diverse, and often effected a change in overall spectral tuning (e.g. panels C,D) including in spectral opponency (e.g. panels F-H). Arrowheads in (F) and (H) highlight wavelength-specific switches in the On-channel that led to a change in colour-opponency.*

ACs exhibit low spectral diversity. We next wondered how the different manifestations of AC-effects on BC spectral processing across the IPL and polarity regimes might reflect colour processing in the ACs themselves. Accordingly, we expressed SyGCaMP3.5 under the ptf1a promoter which targets the vast majority of ACs in zebrafish[44,45] (Figure 7A). We then recorded dendritic calcium responses of ACs to the same battery of stimuli used to probe BCs. ROIs were placed based on local response correlation using previously established analysis pipelines[12,37] (Figure 7B,C, Methods). We recorded from both the acute zone[46] and from the nasal retina and pooled the data (n = 10 scans each). Across the entire dataset ROIs were detected at all IPL depths, and like for BCs, AC-responses tended to occur predominately in two major bands, towards the respective centres of the traditional On- and Off-layers (Supplemental Figure 5).

We next used a Mixture of Gaussian model to cluster ACs based on their function (Methods). This returned 27 clusters, here arranged by IPL depth (Figure 7D-H, cf. Supplemental Figure 5). To what extent these clusters correspond to AC-types remains unknown, and in view of >60 AC types in mice[21], 27 putative types in zebrafish probably underestimates their full diversity. Such possible underestimation is likely part related to the necessarily incomplete sampling of the full stimulus space. Nevertheless, our clusters showcased a substantial response diversity in terms of kinetics and polarities, however notably less so in terms of spectral signals. For example, eight out of ten Off-stratifying AC-clusters ($C_{1\text{-}5,7\text{-}10}$) exhibited Off-responses to the 'white' step of light (Figure 7D). These clusters differed strongly in their temporal properties (Figure 7D), but hardly at all in their spectral tunings (Figure 7E-G). The remaining two Off-stratifying clusters exhibited On-responses ($C_{6,9}$). Next, based on the responses to the "white" step of light, AC-clusters stratifying in the traditional On-layer (C_{11}-C_{27}) were comprised of eleven On-clusters ($C_{11,13\text{-}15,17\text{-}19,23,24,26,27}$), three Off-clusters ($C_{12,20,25}$) and three On-Off-clusters ($C_{16,21,22}$). At the level of kinetics ACs strikingly resembled the corresponding changes observed amongst BCs upon AC-block (Supplemental Figure 8A, cf. Figure 2J), indicating a tight correspondence between these observations.

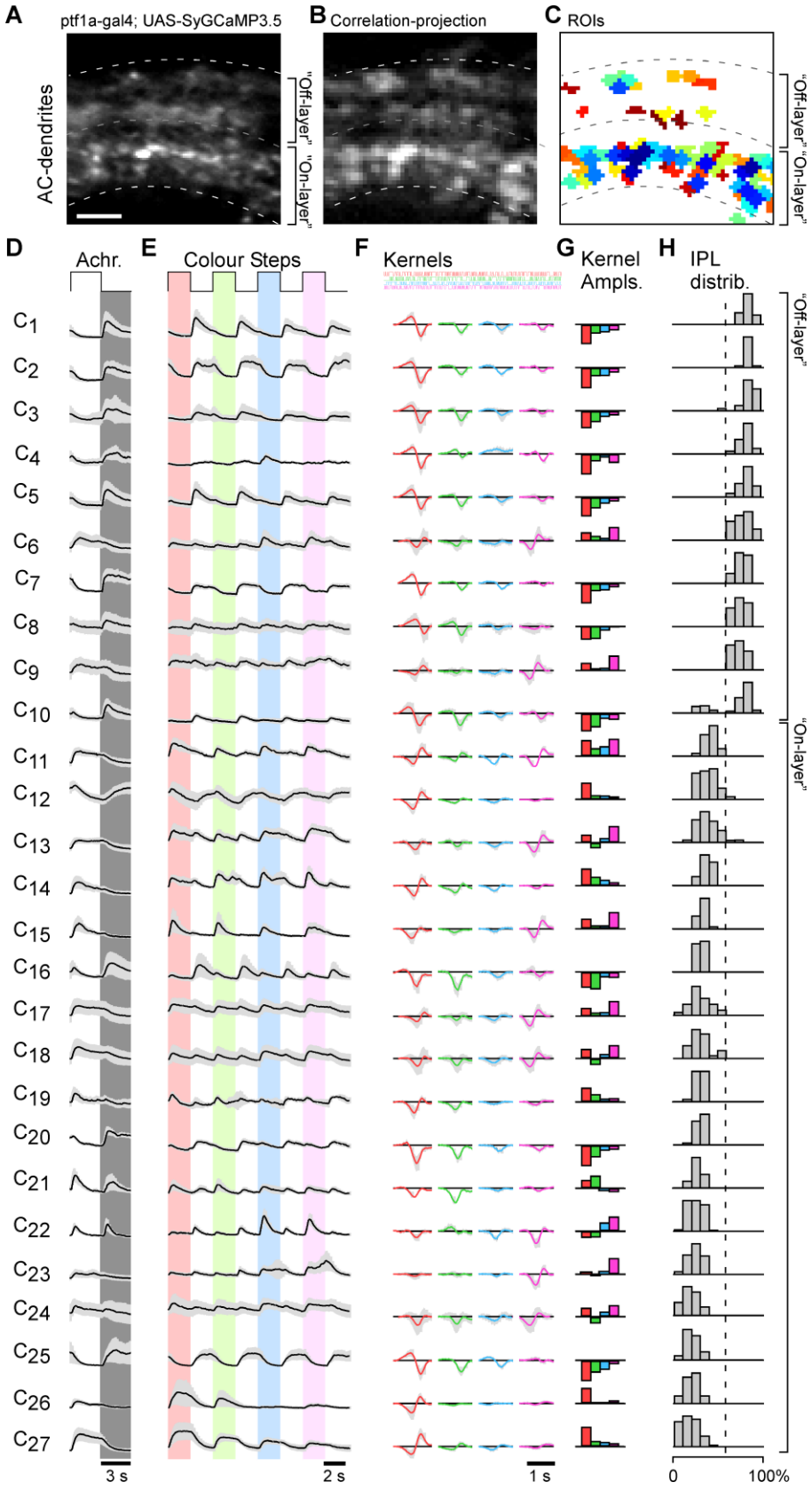

Figure 7 – Spectral processing in ACs. A-C, *Example scan of syGCaMP3.5 expressing AC-dendrites within the IPL, showing the scan average (A), a projection of local response correlation, indicating regions of high activity (B) and the correspondingly placed ROI-map (C).* ***D-H****, Overview of AC-clusters based on the responses of n = 1,743 ROIs in n = 20 scans from n = 6 fish (Methods) to the same battery of stimuli used to probe BC-functions (cf. Figure 1). Shown are the mean±SD of the step in the 'white' chirp (D), the corresponding "colour" steps (E), kernels (F) and their extracted amplitudes (G), and each cluster's distribution across the IPL (H).*

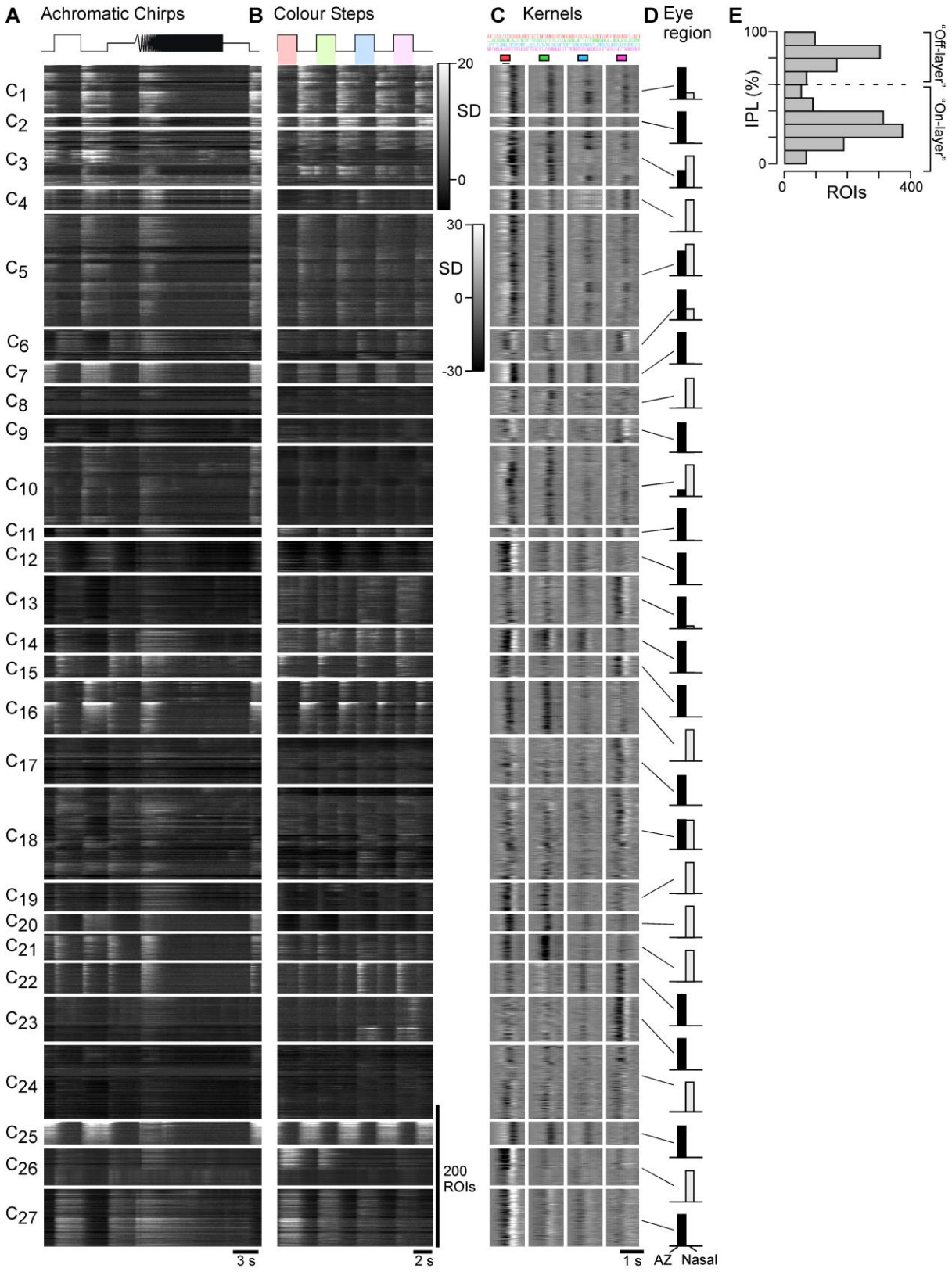

Figure S5 – related to Figure 7. *Detail of AC clusters, showing heatmaps of the full dataset leading to the cluster means shown in Figure 7. Shown are the full chirps (A, note that for simplicity, only the step portion is shown in Figure 7), the "colour" steps (B), the kernels (C) and the eye region of the included ROIs (D, Acute zone or Nasal retina).* ***E****, IPL distribution of all AC-ROIs.*

Next, despite their substantial diversity in terms of polarities and kinetics (Figure 7D), the 27 AC-clusters were readily sorted into only four spectral groups (Figure 8A-D, Methods): two large non-opponent groups (long-biased: $C_{1\text{-}5,7,8,10,12,14,16,19,20,25,\text{-}27}$; "V-shaped": $C_{6,9,11,15,17}$, Figure 8A,B) which together comprised 21 of the 27 clusters, and two small opponent groups which comprised the remaining six (RG/BU: $C_{21,22}$; RBU/G: $C_{13,18,23,24}$, Figure 8C,D). In fact, all eleven Off-clusters, as well as five of the ten On-clusters were spectrally very simple indeed, all falling into the long-wavelength biased non-opponent group (Figure 8A). The remaining five non-opponent On-clusters fell into a second relatively simple group that was spectrally "V-shaped" (Figure 8B). Accordingly, the vast majority of ACs clusters, which included all non-opponent clusters, exhibited only two flavours of spectral responses. These ACs might, therefore, be expected to primarily shape non-spectral BC and/or RGC functions.

The remaining six clusters, which were classed as opponent (Figure 8C,D), all exhibited prominent On-Off responses to at least a subset of the spectral steps (e.g. Figure 8E,F). In all six cases, their opponency resulted from a spectral rebalancing of On- versus Off- amplitudes rather than a "classical" full polarity inversion as in BCs[14]. Taken together, and perhaps surprisingly, from a spectral point of view, ACs were substantially less complex than BCs (Figure 3, see also Refs[14,15]).

AC spectral tunings are mostly explained by inputs from the "achromatic" red- and UV-cones. Based on the spectral simplicity of most AC-clusters, we next wondered to what extent their tuning functions might be explained from the spectral tunings of the cones. In zebrafish, red- and UV-cones are non-opponent, and associated with achromatic processing, while green- and blue-cones are strongly opponent, and associated with "colour" processing[7].

Here, superposition of the different cones' tuning functions on those of ACs strongly hinted that most AC-spectral tunings might be readily explained by inputs from red- and UV-cones alone (shadings in Figure 8A-D). For example, the sixteen long-wavelength-biased AC-clusters were highly reminiscent of red-cones (Figure 8A). Similarly, the five spectrally V-shaped AC-clusters and both RG:BU-opponent clusters were reminiscent of non-opponent (Figure 8B) and opponent (Figure 8C) combinations of red- and UV-cone signals. Only the remaining four RBU:G-opponent clusters appeared to mimic diverse forms of UV- versus green-cone opponencies (Figure 8D).

To quantitatively confirm these matches, we fitted the spectral tuning function of each AC-cluster with those of all four cones, or with various possible subsets thereof (Figure 8G). While, as expected, the best fits were achieved when using all four cones as inputs (on average capturing 97%, 85%, 92% and 88% of the signals amongst the four spectral AC-groups, respectively), only marginally lower quality fits were achieved by substantially simpler cone combinations (Supplemental Figure 6B, Figure 8F,G). For example, restricting inputs to only red- and UV-cones still allowed capturing 86% and 82% of the signals across long-wavelength biased and V-shaped groups, respectively (Figure 8G, red dotted lines). The same restricted model also allowed capturing 91% of the signal in one of the two RG:BU opponent groups (C_{22}).

However, the same strategy could not explain the remaining five opponent clusters, capturing only an average of 58%. Capturing these opponent clusters instead required exchanging red- for green-cone inputs, still alongside UV-cones, capturing 81% signal amongst four RBU:G opponent clusters compared to 88% in the full model (Figure 8G, green dotted lines). The single remaining RG:BU-opponent cluster (C_{21}) remained poorly captured by this strategy (62%); however, this could be restored to 88% by using both red- and green-cones alongside UV (turquoise dotted line).

Taken together, 22 of 27 AC-clusters are therefore reasonably explained by inputs from red- and UV-cones alone, while the remaining five – all opponent – could be

explained by additional inputs from green-cones, either alongside or without red-cones. Blue-cones were generally not required to capture the essence of any ACs' spectral tuning functions. Overall, the spectral simplicity of most ACs, and the apparent predominance of inputs from the two non-opponent cones, supports the idea that zebrafish ACs are not primarily set-up for spectral processing.

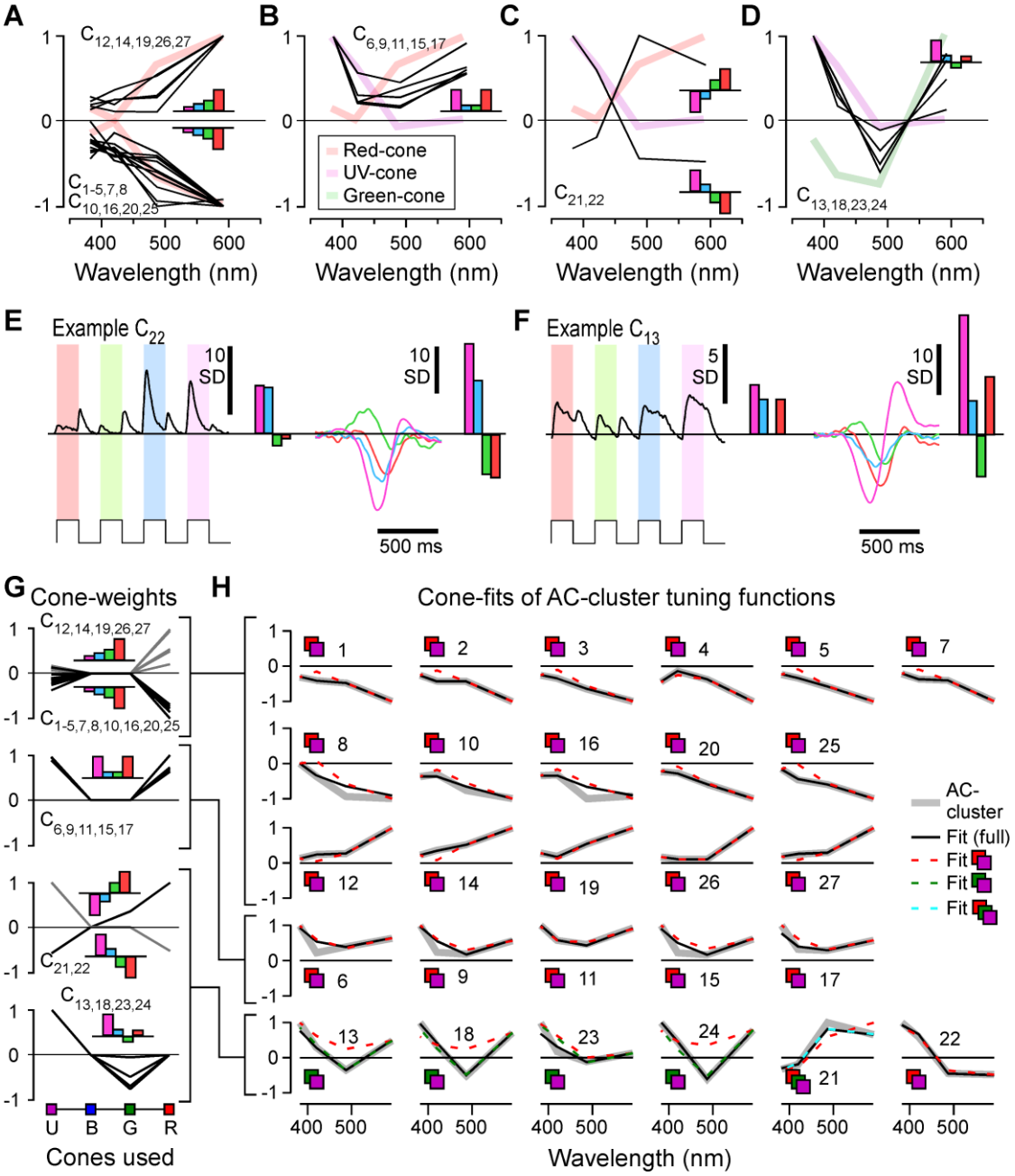

***Figure 8 – spectral processing in ACs. A-D**, Spectral tuning functions of all AC-clusters, allocated to one of four groups as shown: Long-wavelength biased (A), V-shaped (B), long: short opponent (C), and "green-opponent" (D). Plotted behind the AC-spectral tunings are "reduced" tuning functions of selected cones (cf. Supplemental Figure 3D) to illustrate qualitative spectral matches between cones and AC-clusters. **E, F**, Means of "colour" steps and kernels of two selected example clusters that were classed as opponent. Note that in both cases, the opponency arises due to a wavelength-dependent rebalancing of On-Off responses, rather than a "classical" full-polarity reversal. **G,H**, Cone-weights (G) and overview of fits (H) between spectral tuning functions of "reduced" cones (see above) and AC-cluster means. The four plots in (G) correspond to the four spectral groups shown in (A-D). (H) shows one panel per cluster as indicated, sorted by their spectral groups. Shown are: AC-cluster mean (grey, thick), the best fit when using all four cones (black) and the fit result when only using red- and UV-cones (red, dashed). We also show the fit results for the six opponent clusters (bottom row) when using only green- and UV-cones (green, dashed) and when using red-, green- and UV-cones (light blue, dashed). For evaluation of fit qualities, see Supplemental Figure 6B.*

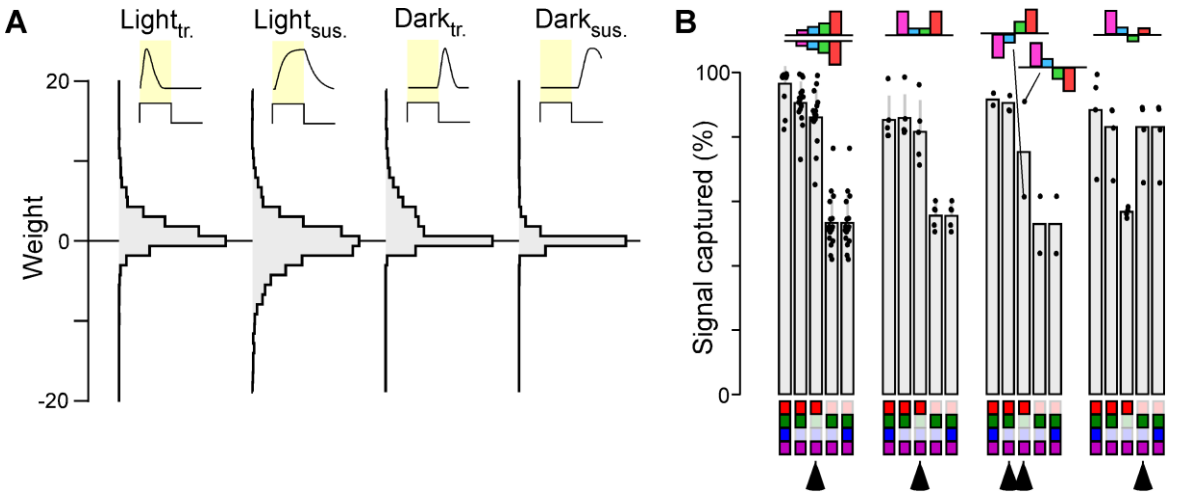

***Figure S6 – related to Figure 8. A**, Summary of kinetic component weights used to fit the 'white' step responses across all AC-ROIs, shown as peak normalised (cf. Figure 2J for BCs). **B**, evaluation of fit quality for the model linking the spectral tuning functions of "reduced" cones with those of AC-cluster means. Shown in each case is the percentage of the AC-clusters' spectral signal captured (as area under the curve) by each fit. The cone-combinations used for each fit are indicated below, and the four spectral groups (cf. Figure 8A-D) plotted separately as indicated. In each case, the best fits allowing for >80% signal capture are indicated by the arrowheads.*

ACs exhibit the highest spectral diversity in the traditional On-layer. Finally, despite the relative spectral simplicity of ACs, our data from BCs shows that at least some ACs must impact inner retinal colour processing. Since most of the spectral tuning amongst BCs occurred in the traditional On-layer of the IPL (Figure 3E-H), we assessed if the ACs might also show their highest spectral diversity in this part of the inner retina. This was indeed the case (Figure 9): while the traditional Off layer was near-exclusively occupied by red-cone-like ACs, alongside a comparatively minor contribution from V-shaped ACs, the On-layer comprised representatives from all spectral AC-groups, including the vast majority of ROIs allocated to any of the six of the colour opponent AC clusters.

We conclude that most spectral interactions between ACs and BCs that contribute towards "dynamically preserving" colour opponency in BCs (Figure 3) occur in the traditional On-layer of the IPL (Figure 9).

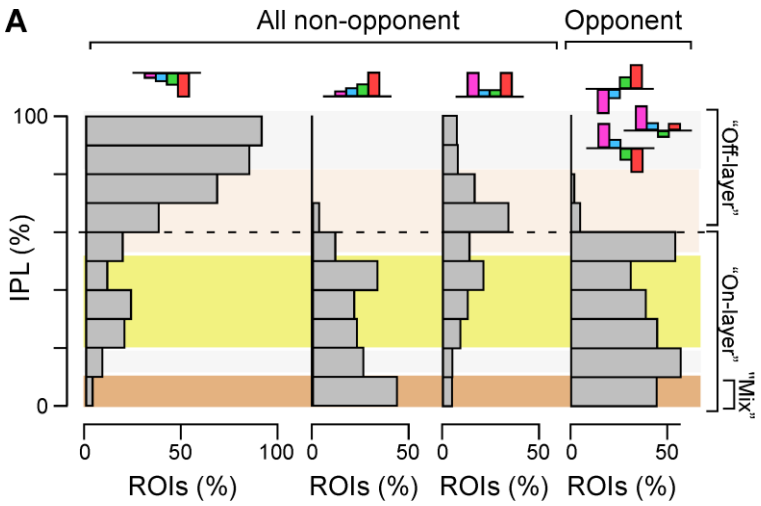

***Figure 9 – The On-layer harbours most spectral diversity among ACs.** IPL-profiles of AC-clusters by spectral group as indicated (cf. Figure 8A-D). Note that the long-biased clusters are divided into "On" and "Off" groups, while the opponent groups are combined. The background shadings correspond to those extracted from BCs (cf. Figure 3E-H).*

DISCUSSION

The role of ACs in colour vision. We have shown that, despite profound impacts of ACs on diverse aspects of light processing in BCs (e.g. Figures 1,2), the population representation of colour opponency was remarkably invariant to pharmacological removal of inner retinal inhibition (Figure 3). This observation implies that ACs are not categorically required for the inner retina's encoding of key "colour information" per se. Rather, BC colour processing appears to function 'in spite of' the pervasive presence of inhibitory networks in the inner retina. To achieve this balance, ACs appear to implement a "switch", by which they mask pre-existing colour opponency in some BCs, while at the same time generating qualitatively equivalent information elsewhere (Figures 3,4). This switch was implemented mostly by On-circuits (Figure 5,6). Correspondingly the dendrites of ACs that exhibit spectral opponency (Figure 7,8) were located in the traditional On-layer (Figure 9). In the future, different anatomical distributions of colour coding BCs in the presence and absence of AC-inputs may provide an important handle for studying the diverse AC-BC circuits that contribute to this overall spectral balancing. Further, understanding if and how these correlative observations are causally linked will likely require the use of more specific transgenic lines that allow more selectively interfering with specific types of BCs and ACs. The same strategy should also help to decipher those BC circuits where ACs mask a pre-existing opponency.

Colour opponency in the absence of ACs. The complex interplay of masked and generated BC opponencies in the absence of inner retinal inhibition directly confirms the expectation that BCs do inherit diverse spectral opponencies from the outer retina[5,7,14]. However, the full picture is decidedly more complex than anticipated from previous work. That long- and mid-wavelength opponencies can be preserved in BCs in the absence of ACs is perhaps expected, since these two axes are already fully represented by the two mid-wavelength cones[7]. However, it remains unclear how the third, short-wavelength opponent axis can persist. While, as with primates[47], zebrafish UV-cones (SWS1) also exhibit weak but significant "UV:yellow" opponency[7], it seems implausible that this can account for the observed effects. First, this pre-existing outer retinal opponency would need to be substantially boosted to match the much more pronounced opponency in BCs (e.g. Figure 3A). Second, in cones, this opponency was restricted to the acute zone, and, therefore, it cannot account for the profusion of BCs' UV:yellow opponencies observed outside this retinal region[14]. Instead, the continued presence of UV:yellow opponency in BCs following AC-block strongly points to the existence of an unknown mechanism capable of selectively inverting cone signals within single BCs. Three putative and non-mutually exclusive mechanisms present themselves. First, a single BC might express both depolarising and hyperpolarising glutamate receptor systems at their dendritic tips that contact different cones. Second, BCs could receive direct inputs from HCs. For example, a putative BC driven by sign-inverted inputs from UV-cones (i.e. "UV-On") could simultaneously receive sign-preserving inputs from H1 and/or H2 HCs, which themselves carry a sign-preserving long-wavelength biased signal[7]. In zebrafish, the presence of direct inputs from HCs to BCs has not been observed; however, the concept is tentatively supported by the anatomical presence HC-BC contacts in mice[48]. Third, zebrafish might have ACs that use "fast" neurotransmitters other than GAGA and/or glycine, which presumably continue to function throughout our pharmacological interventions. For example, mice feature VGlut3 ACs, a population of part-glutamatergic ACs implicated in motion processing[49–51]. Similarly, another key neuron implicated in mammalian motion processing is the starburst amacrine cell (SAC) which co-releases acetylcholine alongside GABA[28,52]. However, the functional role of SACs outside mammals remains sparsely explored[53]. Related, we also cannot exclude the possibility that a subset of GABA- and/or glycinergic interactions between ACs and BCs in zebrafish rely on receptor systems that were not targeted by our drug-cocktail. In the future, it will be important to experimentally test each of these possibilities.

The role of green- and blue-cone circuits in supporting inner retinal colour processing. Unlike red- and UV-cones, zebrafish green- and blue-cones provide strongly colour opponent outputs due to feedforward signals from the HCs[7]. Accordingly, these cones might directly support colour opponency in BCs. In support of this hypothesis, the spectral zero-crossings marked by these two cones remain represented within BCs, both in the presence and in the absence of ACs. However, only a minority of green- and blue-cone-like BCs retained their specific opponency upon AC-block (Figure 3C). This suggests that while the signals from green- and blue- cones can be directly used to support colour opponency in BCs, this motif is by no means dominant when considering the complete circuit. Instead, most BC circuits that represent these two spectral opponencies required inputs from ACs. In zebrafish, green- but not blue-cones provide cone-type-exclusive drive for at least two anatomically distinct types of BCs[11], providing a possible neural substrate for the minority of green-cone-like BCs that were unaffected by AC-block. These might account for some of the unmasked green-cone-like BCs when ACs were blocked (Figure 3C, 4G). Possible green-cone-exclusive BCs might also link with the observation that green-light stimulation could result in long-wavelength biased spectral effects on BCs (Figure 5F), and that most opponent ACs seemed to be partially built from green-cone inputs (Figure 8F).

In contrast, the possible roles of blue-cones in zebrafish colour vision remain much more elusive. A blue-cone-exclusive BC is not known to exist[11], which leaves the origin of any "intrinsic" blue-cone-like BC-tunings unclear (Figure 3C, Figure 4B,H). Further, we found no evidence of any major involvements of blue-cones in AC-processing (Figure 8). On the other hand, the four LEDs used in the present study were not optimally placed to disambiguate blue- from UV-cone contributions (Supplemental Figure 3D). Nevertheless, our findings add to a perhaps puzzling body of evidence that questions a key role of blue-cones in shaping larval zebrafish vision[5].

A special role of On-circuits in zebrafish colour vision? Most AC-mediated spectral tuning in BCs – whether leading to changes in opponency or simply a rebalancing of non-opponent spectral tunings – were predominately implemented via the On- rather than the Off-channel (Figures 5,6,9). This observation adds to a growing body of evidence that zebrafish generally leverage On- rather than Off-circuits to compute diverse aspects of "colour-information". For example, both at the level of the retinal output[37], and within the brain[36,54,55], most spectral diversity is represented in the On-channel. In contrast, the spectral tuning function of the brain's overall Off-response essentially resembles the spectral tuning function of red-cones in isolation, which also corresponds with the mean-spectrum of natural light in the zebrafish natural habitat[7,36]. From here, it is tempting to speculate that zebrafish generally use the Off-channel as an 'achromatic reference', while On-circuits can, where required, provide spectrally biased points of comparison to serve spectral and colour vision.

The predominant use of one rather than both polarities for encoding spectral information could also be advantageous, in that it might permit largely unaltered travel of the red-cones' "true" achromatic signal to the brain: by restricting the bulk of spectral computations to the On-strata of the IPL, circuits within the Off-strata can operate in an essentially achromatic manner. In agreement, the vast majority of ACs in the Off layer exhibited such achromatic tunings (Figure 8A,B). In the future it will be interesting to test if such an On-dominance amongst spectral computations is also a feature in other vertebrates.

A short-wavelength dominance of AC-BC interactions? Perhaps paradoxically, the removal of inner retinal inhibition disproportionally impacted short- over long-wavelength processing in BCs (Figure 5) – even though the majority of AC circuits themselves were long-wavelength dominated (Figure 8). However, this apparent mismatch does become less pronounced when considering On- and Off-circuits in isolation. To a large extent, the long-wavelength bias amongst ACs was driven by the Off-channel. In contrast, the majority of On-ACs did in fact feature pronounced

UV-responses (Figure 8F). The latter might partly account for the observed dominance of UV-modulation amongst BCs, which occurred almost exclusively in the On-channel. The disproportionately high intrinsic gain of the zebrafish's UV-On system[5,46] might further contribute to the observed effects. Finally, it is notable that amongst the many non-opponent ACs, two spectral shapes predominate: one driven mainly by red-cones ("long biased", Figure 8A), and one driven by red- and UV-cones in approximate balance ("V-shaped", Figure 8B). In principle, this arrangement should allow the impartation of a "pure" UV-cone-like effect on BCs by combining inputs from long-wavelength biased Off-ACs with V-shaped On-ACs on a common BC, since red-cone inputs could then cancel.

The origin of On-Off BCs. Blocking ACs unmasked a small (~5%) but highly reproducible fraction of "intrinsic" On-Off responses amongst BCs that were wholly absent during control conditions (Figure 2F). What could be the source of these responses, which were mostly observed in the traditional Off-layer (Figure 2G)? Here, opponency in cones is unlikely to explain this observation. This is because cone-inversions from their "intrinsic" Off-response to an HC-mediated overall On-response occurs exclusively at long-wavelengths[7]; however, the unmasked On-Off BCs were short-wavelength biased (Figure 5A). Instead, as for the observed "intrinsic" UV:yellow opponent BCs (see above), their existence points to the presence of yet unexplained mechanisms of signal transfer between cones and BCs in the zebrafish retina.

Author speculation: An evolutionary perspective. Finally, our results provide tentative insights into the evolution of computation in the brain: in vertebrates and diverse invertebrate eyes alike, the evolution of "colour" computations likely preceded the evolution of complex spatiotemporal vision. This is because (i) opsins including their immediate spectral diversification preceded the evolution of highly resolved spatial vision in any animal by some 200 million years[56], (ii) all extant vertebrates, including lampreys, feature subsets of the same four ancestral opsins across their photoreceptors[4,5], and (iii) particularly in shallow water where vision first evolved, spectral information provides a wealth of behaviourally critical cues that do not categorically need supplementing with spatial information (discussed e.g. in Refs[5,56]). From here, it seems plausible that the earliest forerunners of vertebrate eyes[57] gradually evolved the bulk of their inner retinal circuits on top of well-functioning outer retinal circuits that already provided useful spectral information. In such a scenario, inner retinal circuit evolution would have occurred under constant selection pressure to maintain coding efficiency for colour vision, thus perhaps explaining the arrangement that we see in zebrafish today. This interpretation would further imply that perhaps also in other layered networks of brains, the primary function of some microcircuits may not be to "create new" computations, but rather to make up for computations which would otherwise be lost.

METHODS

Lead Contact

Further information and requests for resources and reagents should be directed to and will be fulfilled by the Lead Contact, Tom Baden (t.baden@sussex.ac.uk).

Data and Code Availability. Pre-processed functional 2-photon imaging data and associated summary statistics will be made freely available on Data Dryad and via the relevant links on http://www.badenlab.org/resources and http://www.retinal-functomics.net.

Materials Availability. The transgenic lines Tg(ribeye:Gal4; UAS:SyGCamp3.5), Tg(ptf1a:Gal4;UAS:SyGCamp3.5) used in this study have been previously published[45] and are also available upon request to the lead author.

EXPERIMENTAL MODEL AND SUBJECT DETAILS

Animals. All procedures were performed in accordance with the UK Animals (Scientific Procedures) act 1986 and approved by the animal welfare committee of the University of Sussex. Animals were housed under a standard 14:10 day/night rhythm and fed three times a day. Animals were grown in 0.1 mM 1-phenyl-2-thiourea (Sigma, P7629) from 1 *dpf* to prevent melanogenesis. For all experiments, we used 6-8 days post fertilization (*dpf*) zebrafish (Danio rerio) larvae. For 2-photon *in-vivo* imaging, zebrafish larvae were immobilised in 3% low melting point agarose (Fisher Scientific, BP1360-100), placed on a glass coverslip and submerged in fish water. Eye movements were prevented by injection of α-bungarotoxin (1 nL of 2 mg/ml; Tocris, Cat: 2133) into the ocular muscles behind the eye. For pharmacological AC blockage, we injected ~4 nL of a solution containing antagonist to $GABA_A$, $GABA_C$ and glycine receptors into the anterior chamber of the retina. The estimated final concentration in the extracellular space was 5 µM gabazine (Sigma) as antagonist of $GABA_A$ receptors; 5 µM TPMPA (Sigma) as antagonist of $GABA_C$ receptors; 5 µM strychnine (Sigma) as antagonist of glycine receptors[38]. The solution also contained 1 mM Alexa 594 for verifying the quality of the injection.

METHOD DETAILS

***Light Stimulation*.** With fish mounted on their side with one eye facing upwards towards the objective, light stimulation was delivered as full-field flashes of light. For this, we focused a custom-built stimulator through the objective, fitted with band-pass-filtered light-emitting diodes (LEDs) ('red' 588 nm, B5B-434-TY, 13.5 cd, 8˚; 'green' 477 nm, RLS-5B475-S, 3-4cd, 15˚, 20 mA; 'blue' 415 nm, VL415-5-15, 10-16 mW, 15˚, 20 mA; 'ultraviolet' 365 nm, LED365-06Z, 5.5 mW, 4˚, 20 mA; Roithner, Germany). LEDs were filtered and combined using FF01-370/36, T450/pxr, ET420/40 m, T400LP, ET480/40x, H560LPXR (AHF/Chroma). The final spectra approximated the peak spectral sensitivity of zebrafish R-, G-, B-, and UV-opsins (Supplemental Figure S3B-D), respectively, while avoiding the microscope's two detection bands for GFP and mCherry. To prevent interference of the stimulation light with the optical recording, LEDs were synchronized with the scan retrace at 1 kHz (1 ms line duration) using a microcontroller and custom scripts. Further information on the stimulator, including all files and detailed build instructions can be found in Ref[35].
Stimulator intensity was calibrated to be spectrally flat at 30 mW per LED, which corresponds to low-photopic conditions. Owing to 2-photon excitation of photopigments, an additional constant background illumination of ~10^4 R^* was present throughout[66,67]. For all experiments, larvae were kept at constant illumination for at least 5 seconds after the laser scanning started before light stimuli were presented. Three types of full-field stimuli were used: (i) a spectrally flat 'white' chirp stimulus[68] where all four LEDs were driven together, (ii) flashes of light at each of the four wavelengths (2 s On, 2 s Off), and (iii) a binary dense and spectrally flat white noise, in which the four LEDs were flickered independently in a known random binary sequence at 6.4 Hz for 300 seconds.

***2-photon calcium imaging*.** All 2-photon (2P) imaging was performed on custom-built 2P microscope equipped with a mode-locked Ti:Sapphire laser (Chameleon 2, Coherent) tuned to 915 nm for SyGCaMP3.5 imaging. Emitted photons were collected through the objective (Nikon, MRD77225, 25X) as well as through an oil condenser (NA 1.4, Olympus) below the sample using GaAsP photodetectors (H10770PA-40, Hamamatsu). For image acquisition, we used ScanImage software (r 3.8) running under Matlab (R 2013b). All recordings were taken at 128 x 100 pixels (10 Hz frame rate at 1 ms per scan line).

Data analysis. Data analysis was performed using IGOR Pro 6.3 (Wavemetrics), Fiji (NIH) and Matlab R2019b / R2020b (Mathworks).

ROI placement, IPL detection and functional data pre-processing. Where necessary, images were xy-registered using the registration function provided in SARFIA[69] running under IGOR Pro 6.3. For BC data, regions of interest (ROIs) were drawn by hand based on the standard deviation projection across the tetrachromatic noise data. The ROIs from control condition and drug condition were drawn separately. Terminals were "paired" across the two conditions using the experimenter's best judgment, which we found to be more reliable than automated procedures. The matching of terminals across conditions was greatly facilitated by the sparse expression strategy, and throughout we tried to be as conservative as possible to only match terminals when we were certain that they are the same ones (i.e. minimising false positives, at the expense of false negatives). For AC data, ROIs were defined automatically based on local image correlation over time, as shown previously[12].

In all scans, IPL boundaries were drawn by hand using the custom tracing tools provided in SARFIA[69]. The IPL positions were then determined based on the relative distance of a ROIs' centre of mass between the IPL boundaries and mapped to the range 0% to 100%.

Fluorescence traces for each ROI were z-normalised, using the time interval 2-6 seconds at the beginning of recordings as baseline. A stimulus time marker embedded in the recording data served to align the Ca^{2+} traces relative to the visual stimulus with a temporal precision of 1 ms. Responses to the chirp and step stimuli were up-sampled to 1 kHz and averaged over 5 trials. For data from tetrachromatic noise stimulation we mapped linear receptive fields of each ROI by computing the Ca^{2+} transient-triggered-average. To this end, we resampled the time-derivative of each trace to match the stimulus-alignment rate of 500 Hz and used thresholding above 0.7 standard deviations relative to the baseline noise to the times t_i at which Calcium transients occurred. We then computed the Ca^{2+} transient-triggered average stimulus, weighting each sample by the steepness of the transient:

$$\boldsymbol{F}(l,\tau) = \frac{1}{M}\sum_{i=1}^{M} \dot{\boldsymbol{c}}(t_i)\boldsymbol{S}(o, t_i + \tau)$$

Here, $\boldsymbol{S}(l,t)$ is the stimulus ("LED" and "time"), τ is the time lag (ranging from approx. -1,000 to 350 ms) and M is the number of Ca^{2+} events. The resulting kernels are shown in z-scores for each LED, normalised to the first 50 ms of the time-lag. To select ROIs with a non-random temporal kernel, we used all ROIs that exceeded a standard deviation of ten in at least one of the four spectral kernels. The precise choice of this quality criterion had no major effect on the results.

***Kernel polarity*.** The use of a fluorescence-response-triggered average stimulus (here: 'kernel') as a shorthand for a neuron's stimulus-response properties, while potentially powerful (e.g. Refs[12,15,37]), ought to be considered with some caution. For example, determining a binary value for a kernel's polarity (On or Off) can be conflicted with the fact that a neuron might exhibit both On and Off response aspects. Moreover, different possible measures of On or Off dominance in a kernel can generate different classification biases. Here, following our previously established approach[15,37] we defined On and Off based on a measure of a kernel's dominant trajectory in time. Before the calculation, we first smoothed the kernels to eliminate the high-frequency noise. After that, we determined the position in time of each kernel's maximum and minimum. If the maximum preceded the minimum, the kernel was classified as Off, while vice versa if the minimum preceded the maximum, the kernel was defined as On.

Reconstruction of step responses using kinetic components. To reconstruct each cell's mean response into constituent spectral and temporal components we used four temporal components associated with a given light response (i.e. 3 s light, 3 s dark for 'white' steps, and 2 s light 2 s dark for 'colour' steps), following a previously described approach[14]. The temporal components used resembled light-

transient, light-sustained, dark-transient, and dark-sustained temporal profiles (Figure 2B, S5C). These components were fitted to the trial-averaged step responses of individual ROIs in sequence, in each case minimising the mean squared difference between a template's peak and the corresponding five time-points in measured response, with previously fitted components subtracted. The fit sequence was: Light-sustained, light-transient, dark-sustained, dark-transient. This yielded four corresponding weights, scaled in z-scores in accordance with the amplitudes of the trial averaged response means. To assess reconstruction quality (Supplemental Figure S2A,B and S4E,F), reconstructed data was subtracted from the original ROI-means to yield residuals. From here, we compared original data, reconstructions, and residuals based on variance explained across all ROIs (as in Ref[14]). To this end, we first computed the total variance across all clusters for each time-point. The result of this process, plotted beneath each corresponding heatmap showed similar time-variance profiles across cluster means and their reconstructions (panels 1 and 2), but very little remaining signal for the residuals (panel 3). From here, we computed the area under the curve for each variance-trace and normalised each to the result from the original cluster means. By this metric, reconstructions captured 98%, 97%, 95% and 96% of the total variance for the 'white-control', 'white-AC-block' and 'colour-control' and 'colour-AC-block' steps, respectively.

Response polarity per ROI was then computed as follows. A ROI was considered as displaying an On-response if the sum of the light-transient and light-sustained weights exceeded 3 SD. A ROI was considered as displaying an Off-response if either the sum of the light-transient and light-sustained weights was more negative than -3 SD, or if the sum of the dark-transient and dark-sustained components exceeded 3 SD. If by these criteria a ROI display both On- and Off-responses, it was counted as On-Off. ROIs failing to elicit either On- or Off-responses were counted as non-responsive. Finally, for simplicity we also consolidated the four kinetic weights associated with a given step into a single 'compound weight' (shown, for example, for all colour steps). This was done by summing all weights, with those of dark components inverted.

Relating kernels and "colour" steps. We probed BC and AC spectral tuning in two complementary ways: by presenting "colour" steps from dark, and via the "colour" kernels. Here, we reasoned that while the spectral steps and the kernels could both provide useful insight into this question, the kernels were likely more representative of BCs' full spectral response because they measured BC sensitivities against a grey rather than a black background. The kernels also tended to accentuate spectral differences compared to the steps, possibly because the spectral channels were probed simultaneously rather than in sequence. Nevertheless, the results from steps and kernels were generally in good agreement with each other. The polarities estimated by either method mismatched in only 1% of cases, compared to 61% matches (Supplemental Figure 4H). The remaining 38% of correspondences stemmed from cases when either the step-responses (25%) or the kernels (12%) did not pass our minimum response criterion. Accordingly, by using the kernels rather than the spectral steps, we could also draw on a larger fraction of 'responsive' BCs. Finally, kernels could by definition never be On-Off, but instead revealed either a null-response (e.g. if On- and Off-inputs were approximately balanced), or became either On- or Off- if one of the two polarities predominated, thereby simplifying further analysis. However, for the same set of reasons, the steps were more suited to investigate the spectral differences across On and Off-channels.

Response Synchronisation. To determine the degree of response synchronisation within each scan, we used the synchrony measurement method described in Ref[42], using the z-normalized fluorescence traces from tetrachromatic noise stimulation of the BC data as the input. We first evaluated $F(t)$ across all the recorded terminals within one field of view at a given time t :

$$F(t) = \frac{1}{N}\sum_{i=1}^{N} F_i(t).$$

The variance of the time fluctuations of *F(t)* is

$$\sigma_F^2 = \langle [F(t)]^2 \rangle_t - [\langle F(t) \rangle_t]^2$$

Where $\langle \dots \rangle_t$ denotes the time-averaging over the session. For each terminal $F_i(t)$, we used similar approach to calculate the time fluctuations

$$\sigma_{F_i}^2 = \langle [F_i(t)]^2 \rangle_t - [\langle F_i(t) \rangle_t]^2$$

The synchrony measure, $\chi(N)$, for the scan filed is then calculated as

$$\chi(N) = \sqrt{\frac{\sigma_F^2}{\frac{1}{N}\sum_{i=1}^{N} \sigma_{F_i}^2}}$$

The value of $\chi(N)$ ranges between 0 and 1. $\chi(N) = 1$ indicates that all ROIs within a scan are perfectly synchronized.

Clustering of ACs. Clustering was performed on the dataset containing the functional responses of ACs to chirps, "colour" steps and kernels derived from the colour noise stimulus. All input traces were up-sampled to 1 kHz (cf. pre-processing) which yielded n = 25,000 points (chirp), four times n = 4,000 points (steps) and four times n = 1299 points (kernels). Responses to all three stimuli were used for the clustering.

Regions of interest (ROIs) with low-quality responses to all three stimuli were identified and removed from the data set, ROIs with a high-quality response to at least one stimulus being retained in all cases. The quality of response to the chirp and step stimuli was determined using the signal-to-noise ratio quality index: $QI = Var[\langle \boldsymbol{C} \rangle_r]_t / \langle Var[\boldsymbol{C}]_t \rangle_r$, where C is the T by R response matrix (time samples by stimulus repetitions), and $\langle \cdot \rangle_x$ and $Var[\cdot]_x$ denote the mean and variance respectively across the indicated dimension, $x \in \{r, t\}$ (see Ref[68]). A quality threshold of 0.35 was chosen, below which chirp and step responses were judged to be of poor quality. We calculated the standard deviation in the light intensity over time for each stimulus colour in the kernel (R, G, B and UV). The kernel quality of each ROI was defined as the maximum standard deviation across the four colours. A kernel quality threshold of 5 was chosen, below which kernels were judged to be of poor quality. The raw data set was of size n = 1776. Following quality control, the data set was of size: n = 1743 (98.1% (3 s.f.) of the original).

We scaled the data corresponding to each chirp, step colour and kernel colour by dividing each one by the standard deviation through time and across ROIs. In this way we ensured an even weighting between stimuli.

We used principal component analysis (PCA) to reduce the dimensions of the problem prior to clustering. PCA was performed using the Matlab routine **pca** (default settings). We applied PCA separately to the chirps and to the portions of a data set corresponding to each of the step and kernel colours, retaining the minimum number of principal components necessary to explain ≥99% of the variance. The resulting nine 'scores' matrices were then concatenated into a single matrix ready for clustering. The following numbers of principal components were used – chirp: 41; step: 8 R components, 9 G components, 13 B components and

13 UV components; kernels: 7 R components, 16 G components, 31 B components and 21 UV components, giving 159 PCA components in total.

We clustered the combined 'scores' matrix using Gaussian Mixture Model (GMM) clustering, performed using the Matlab routine **fitgmdist**. We clustered the data into clusters of sizes 1,2,…,50, using i) shared-diagonal, ii) unshared-diagonal, iii) shared-full and iv) unshared-full covariance matrices, such that (50*4 =) 200 different clustering options were explored in total. For each clustering option 20 replicates were calculated (each with a different set of initial values) and the replicate with the largest loglikelihood chosen. A regularisation value of 10^{-5} was chosen to ensure that the estimated covariance matrices were positive definite, while the maximum number of iterations was set at 10^4. All other **fitgmdist** settings were set to their default values.

The optimum clustering was judged to be that which minimised the Bayesian information criterion (BIC), which balances the explanatory power of the model (loglikelihood) with model complexity (number of parameters). Lastly, clusters with <10 members were removed.

Using the above procedure, we obtained 23 clusters (1 cluster with <10 members was removed), with unshared diagonal covariance matrices providing the optimal solution. Finally, we split n = 4 clusters with a notably bimodal IPL distribution into their "On-" and "Off-stratifying" components (IPL-cut at 60% depth), yielding a total of 27 response groups.

***Sorting BCs and ACs into spectral groups*.** Using the computed amplitudes of the four kernels (see above), BCs were sorted into one of nine spectral groups (cf. Figure 3A) as follows. First, all BCs that failed to exceed a minimum absolute amplitude of 10 SD in at least one of the four kernels was counted as non-responsive (group 1). Next, we divided the remaining BCs into non-opponent (groups 2-6) and opponent types (groups 7-9) based on the relative signs of all four (R, G, B, U) kernels. From here, the two sets of BCs were sorted further as follows: *Non-opponent BCs*, in order: Long-biased if *abs*(R+G)>*abs*(B+U)*2, Short-biased if *abs*(R+G)<*abs*(B+U), Mid-biased if *abs*(G+B)>*abs*(R+U)*2, V-shaped if *abs*(R+U)>*abs*(G+B)*2, else: "Broad". Opponent BCs; Short-opponent if (R+G>0 && U<0) || (R+G<0 && U>0), Mid-opponent if (R>0 && B<0) || R<0 && B>0), Long-opponent if (R>0 && G<0) || (R<0 && G>0). Finally, in rare cases where (R>0 && G<0 && U>0) || (R<0 && G>0 && U<0), BCs were allocated as long-opponent if *abs*(R)>*abs*(U) but as short-opponent if *abs*(R)<*abs*(U). ACs cluster means were sorted by the same set of criteria, with the exception that opponent groups were divided into different variants. Specifically, ACs were sorted into the RG:BU and R:GBU groups based on the relative signs of G versus U. Note that despite the otherwise identical sorting procedure compared to BCs, ACs only fell into 4 groups (Figure 8A-D).

Fitting of AC-cluster spectral tuning functions with cones. Spectral tuning functions of AC clusters means were matched to those of previously recorded cones (cf. Supplemental Figure 3C,D) based on the four relative kernel amplitudes (as shown in Figure 8A-D). Fitting was done as follows: For each tested cone-combination (e.g. all cones, or R+U only, etc.) we computed 10^6 possible combined tunings at random by summing the respective "reduced" cone tuning functions (Supplemental Figure 3D) with random scaling between -1 and 1 each. We then computed the linear correlation coefficient between each AC-cluster's tuning function, and each of the randomly generated combined cone-tunings, in each case choosing cone-combination that gave the maximal correlation as the best fit. Finally, for each best fit, we scaled all cone weights to minimise the residual between the corresponding AC-cluster's tuning function and that of the combined cone-tuning.

QUANTIFICATION AND STATISTICAL ANALYSIS

Statistics. No statistical methods were used to predetermine sample size. Owing to the exploratory nature of our study, we did not use randomization or blinding. Wilcoxon signed-rank tests were used for the following datasets: synchronicity of BC activity (Figure 1H, S1H); weights from 'white' steps (Figure 2J); weights from colour steps (Figure 5B); amplitude changes for each colour combination (Figure 5C-F). Wilcoxon rank sum tests were used for the following datasets: green-cone responses between the two conditions (Figure S1K); difference of transient and sustained weights in white steps (Figure S2D). Chi-square tests were used for the following datasets: polarity based on white step stimulation (Figure 2F,H for "all data", Figure 2I for "paired data"); spectral response types based on kernels (Figure 3A,B for "all data", Figure 3C for "paired data"); polarity based on colour steps (Figure 5A).

REFERENCES

1. Land, M.F., and Nilsson, D.-E. (2012). Animal Eyes (Oxford University Press).
2. Sterling, P., and Laughlin, S. (2015). Principles of neural design (The MIT Press).
3. Wässle, H. (2004). Parallel processing in the mammalian retina. Nat. Rev. Neurosci. *5*, 747–57.
4. Baden, T., Euler, T., and Berens, P. (2020). Understanding the retinal basis of vision across species. Nat. Rev. Neurosci. *21*.
5. Baden, T. (2021). Circuit-mechanisms for colour vision in zebrafish. Curr. Biol. *31*, PR807-R80.
6. Gollisch, T., and Meister, M. (2009). Review Eye Smarter than Scientists Believed : Neural Computations in Circuits of the Retina. Neuron *65*, 150–164.
7. Yoshimatsu, T., Bartel, P., Schröder, C., Janiak, F.K., St-Pierre, F., Berens, P., and Baden, T. (2021). Ancestral circuits for vertebrate color vision emerge at the first retinal synapse. Sci. Adv. *7*, 6815–6828.
8. Simoncelli, E.P., and Olshausen, B.A. (2001). Natural image statistics and neural representation. Annu Rev Neurosci *24*, 1193–1216.
9. Buchsbaum, G., and Gottschalk, A. (1983). Trichromacy, opponent colours coding and optimum colour information transmission in the retina. Proc. R. Soc. Lond. B. Biol. Sci. *220*, 89–113.
10. Barlow, H.B.H. (1961). Possible principles underlying the transformation of sensory messages. In Sensory Communication, pp. 217–234.
11. Li, Y.N., Tsujimura, T., Kawamura, S., and Dowling, J.E. (2012). Bipolar cell-photoreceptor connectivity in the zebrafish (Danio rerio) retina. J. Comp. Neurol. *520*, 3786–3802.
12. Franke, K., Berens, P., Schubert, T., Bethge, M., Euler, T., and Baden, T. (2017). Inhibition decorrelates visual feature representations in the inner retina. Nature *542*, 439–444.
13. Franke, K., and Baden, T. (2017). General features of inhibition in the inner retina. J. Physiol. *595*, 5507–5515.
14. Bartel, P., Yoshimatsu, T., Janiak, F.K., and Baden, T. (2021). Spectral inference reveals principal cone-integration rules of the zebrafish inner retina. Curr. Biol. *0*.
15. Zimmermann, M.J.Y., Nevala, N.E., Yoshimatsu, T., Osorio, D., Nilsson, D.-E., Berens, P., and Baden, T. (2018). Zebrafish Differentially Process Color across Visual Space to Match Natural Scenes. Curr. Biol. *28*, 2018-2032.e5.
16. Diamond, J.S. (2017). Inhibitory Interneurons in the Retina: Types, Circuitry, and Function. Annu. Rev. Vis. Sci. *3*, 1–24.
17. Moya-Díaz, J., James, B., Esposti, F., Johnston, J., and Lagnado, L. (2021). Diurnal modulation of multivesicular release controls the efficiency of information transmission at a sensory synapse. bioRxiv, 2021.09.12.459944.
18. Jadzinsky, P.D., and Baccus, S.A. (2013). Transformation of Visual Signals by Inhibitory Interneurons in Retinal Circuits. Annu. Rev. Neurosci. *36*, 403–428.
19. Masland, R.H. (2012). The tasks of amacrine cells. Vis Neurosci *29*, 3–9.
20. MacNeil, M.A., and Masland, R.H. (1998). Extreme diversity among amacrine cells: Implications for function. Neuron *20*, 971–982.
21. Yan, W., Laboulaye, M.A., Tran, N.M., Whitney, I.E., Benhar, I., and Sanes, J.R. (2020). Mouse Retinal Cell Atlas: Molecular Identification of over Sixty Amacrine Cell Types. J. Neurosci. *40*, 5177–5195.
22. Behrens, C., Schubert, T., Haverkamp, S., Euler, T., Berens, P., Baden, T., Schubert, T., Chang, L., Wei, T., Zaichuk, M., et al. (2016). Connectivity map of bipolar cells and photoreceptors in the mouse retina. Elife *5*, 1206–1217.
23. Tanimoto, N., Sothilingam, V., Euler, T., Ruth, P., Seeliger, M.W., and Schubert, T. (2012). BK channels mediate pathway-specific modulation of visual signals in the in vivo mouse retina. J. Neurosci. *32*, 4861–6.
24. Grimes, W.N., Zhang, J., Graydon, C.W., Kachar, B., and Diamond, J.S. (2010). Retinal parallel processors: more than 100 independent microcircuits operate within a single interneuron. Neuron *65*, 873–85.
25. Torvund, M.M., Ma, T.S., Connaughton, V.P., Ono, F., and Nelson, R.F. (2017). Cone signals in monostratified and bistratified amacrine cells of adult zebrafish retina. J. Comp. Neurol. *525*, 1532–1557.
26. Patterson, S.S., Kuchenbecker, J.A., Anderson, J.R., Neitz, M., and Neitz, J. (2020). A Color Vision Circuit for Non-Image-Forming Vision in the Primate Retina. Curr. Biol. *30*, 1269-1274.e2.
27. Lebedev, D.S., and Marshak, D.W. (2007). Amacrine cell contributions to red-green color opponency in central primate retina: A model study. Vis. Neurosci. *24*, 535–547.
28. Famiglietti (1983). "Starburst" amacrine cells and cholinergic neurons: mirror-symmetric on and off amacrine cells of rabbit retina. Brain Res *261*, 138–144.
29. Demb, J.B., and Singer, J.H. (2012). Intrinsic properties and functional circuitry of the AII amacrine cell. Vis. Neurosci. *29*, 51–60.
30. Hsiang, J.C., Johnson, K.P., Madisen, L., Zeng, H., and Kerschensteiner, D. (2017). Local processing in neurites of VGluT3-expressing amacrine cells differentially organizes visual information. Elife *6*.
31. Antinucci, P., Suleyman, O., Monfries, C., and Hindges, R. (2016). Neural Mechanisms Generating Orientation Selectivity in the Retina. Curr. Biol. *26*, 1802–1815.

32. Euler, T., Detwiler, P.B., and Denk, W. (2002). Directionally selective calcium signals in dendrites of starburst amacrine cells. Nature *418*, 845–52.
33. Baden, T., and Osorio, D. (2019). The Retinal Basis of Vertebrate Color Vision. Annu. Rev. Vis. Sci. *5*, 177–200.
34. Dreosti, E., Odermatt, B., Dorostkar, M.M., and Lagnado, L. (2009). A genetically encoded reporter of synaptic activity in vivo. Nat. Methods *6*, 883–9.
35. Zimmermann, M.J.Y., Maia Chagas, A., Bartel, P., Pop, S., Prieto-Godino, L.L., and Baden, T. (2020). LED Zappelin': An open source LED controller for arbitrary spectrum visual stimulation and optogenetics during 2-photon imaging. HardwareX.
36. Bartel, P., Janiak, F.K., Osorio, D., and Baden, T. (2021). Colourfulness as a possible measure of object proximity in the larval zebrafish brain. Curr. Biol. *31*, R235–R236.
37. Zhou, M., Bear, J., Roberts, P.A., Janiak, F.K., Semmelhack, J., Yoshimatsu, T., and Baden, T. (2020). Zebrafish Retinal Ganglion Cells Asymmetrically Encode Spectral and Temporal Information across Visual Space. Curr. Biol. *30*, 2927-2942.e7.
38. Johnston, J., Seibel, S.-H., Darnet, L.S.A., Renninger, S., Orger, M., and Lagnado, L. (2019). A Retinal Circuit Generating a Dynamic Predictive Code for Oriented Features. Neuron *102*, 1211-1222.e3.
39. Robles, E., Laurell, E., and Baier, H. (2014). The Retinal Projectome Reveals Brain-Area-Specific Visual Representations Generated by Ganglion Cell Diversity. Curr. Biol. *24*, 2085–2096.
40. Baden, T., Nikolaev, A., Esposti, F., Dreosti, E., Odermatt, B., and Lagnado, L. (2014). A Synaptic Mechanism for Temporal Filtering of Visual Signals. PLoS Biol. *12*, e1001972.
41. Nirenberg, S., and Meister, M. (1997). THE LIGHT RESPONSE OF RETINAL GANGLION CELLS IS TRUNCATED BY A DISPLACED AMACRINE CIRCUIT. Neuron *18*, 637–650.
42. Golomb, D., and Hansel, D. (2000). The number of synaptic inputs and the synchrony of large, sparse neuronal networks. Neural Comput. *12*, 1095–1139.
43. Westheimer, G. (2007). The ON-OFF dichotomy in visual processing: From receptors to perception. Prog. Retin. Eye Res. *26*, 636–648.
44. Jusuf, P.R., and Harris, W.A. (2009). Ptf1a is expressed transiently in all types of amacrine cells in the embryonic zebrafish retina. Neural Dev.
45. Nikolaev, A., Leung, K.-M., Odermatt, B., and Lagnado, L. (2013). Synaptic mechanisms of adaptation and sensitization in the retina. Nat. Neurosci. *16*, 934–41.
46. Yoshimatsu, T., Schröder, C., Nevala, N.E., Berens, P., and Baden, T. (2020). Fovea-like Photoreceptor Specializations Underlie Single UV Cone Driven Prey-Capture Behavior in Zebrafish. Neuron *107*, 320-337.e6.
47. Packer, O.S., Verweij, J., Li, P.H., Schnapf, J.L., and Dacey, D.M. (2010). Blue-yellow opponency in primate S cone photoreceptors. J. Neurosci. *30*, 568–572.
48. Behrens, C., Yadav, S.C., Korympidou, M.M., Zhang, Y., Haverkamp, S., Irsen, S., Schaedler, A., Lu, X., Liu, Z., Lause, J., et al. (2021). Retinal horizontal cells use different synaptic sites for global feedforward and local feedback signaling. Curr. Biol.
49. Haverkamp, S., Wassle, H., and Wässle, H. (2004). Characterization of an amacrine cell type of the mammalian retina immunoreactive for vesicular glutamate transporter 3. J. Comp. Neurol. *468*, 251–63.
50. Kim, T., Soto, F., and Kerschensteiner, D. (2015). An excitatory amacrine cell detects object motion and provides feature-selective input to ganglion cells in the mouse retina. Elife *4*, e08025.
51. Lee, S., Zhang, Y., Chen, M., Zhou, Z.J.J.Z.J., Amthor, F.R., Takahashi, E.S., Oyster, C.W., Chiao, C.C., Masland, R.H., Fremeau, R.T., et al. (2016). Segregated Glycine-Glutamate Co-transmission from vGluT3 Amacrine Cells to Contrast-Suppressed and Contrast-Enhanced Retinal Circuits. Neuron *90*, 27–34.
52. Lee, S., Kim, K., and Zhou, Z.J. (2010). Role of ACh-GABA cotransmission in detecting image motion and motion direction. Neuron *68*, 1159–72.
53. Euler, T., and Baden, T. (2016). Computational neuroscience: Species-specific motion detectors. Nature *535*.
54. Fornetto, C., Tiso, N., Pavone, F.S., and Vanzi, F. (2020). Colored visual stimuli evoke spectrally tuned neuronal responses across the central nervous system of zebrafish larvae. BMC Biol. *18*, 1–17.
55. Guggiana Nilo, D.A., Riegler, C., Hübener, M., and Engert, F. (2021). Distributed chromatic processing at the interface between retina and brain in the larval zebrafish. Curr. Biol., S0960-9822(21)00153–6.
56. Nilsson, D.-E. (2021). The Diversity of Eyes and Vision. Annu. Rev. Vis. Sci. *7*.
57. Lamb, T.D., Collin, S.P., Pugh, E.N., and Jr (2007). Evolution of the vertebrate eye: Opsins, photoreceptors, retina and eye cup. Nat. Rev. Neurosci. *8*, 960–976.
58. Baden, T., Euler, T., and Berens, P. (2020). Understanding the retinal basis of vision across species. Nat. Rev. Neurosci. *21*, 5–20.
59. Branchek, T., and Bremiller, R. (1984). The development of photoreceptors in the zebrafish, Brachydanio rerio. I. Structure. J. Comp. Neurol. *224*, 107–115.
60. Bilotta, J., Saszik, S., and Sutherland, S.E. Rod contributions to the electroretinogram of the dark-adapted developing zebrafish. Dev. Dyn. *222*, 564–570.
61. Chapot, C.A., Euler, T., and Schubert, T. (2017). How do horizontal cells 'talk' to cone photoreceptors? Different levels of complexity at the cone-horizontal cell synapse. J. Physiol. *595*, 5495–5506.
62. Klaassen, L.J., de Graaff, W., Van Asselt, J.B., Klooster, J., and Kamermans, M. (2016). Specific connectivity between photoreceptors and horizontal cells in the zebrafish retina. J. Neurophysiol. *116*, 2799–2814.
63. Meier, A., Nelson, R., and Connaughton, V.P. (2018). Color Processing in Zebrafish Retina. Front. Cell. Neurosci. *12*, 1–19.
64. Connaughton, V.P., Graham, D., and Nelson, R. (2004). Identification and morphological classification of horizontal, bipolar, and amacrine cells within the zebrafish retina. J. Comp. Neurol. *477*, 371–385.
65. Euler, T., Haverkamp, S., Schubert, T., and Baden, T. (2014). Retinal Bipolar Cells: Elementary Building Blocks of Vision. Nat. Rev. Neurosci. *15*, 507–519.
66. Euler, T., Hausselt, S.E., Margolis, D.J., Breuninger, T., Castell, X., Detwiler, P.B., and Denk, W. (2009). Eyecup scope--optical recordings of light stimulus-evoked fluorescence signals in the retina. Pflugers Arch. *457*, 1393–414.
67. Euler, T., Franke, K., and Baden, T. (2019). Studying a light sensor with light: Multiphoton imaging in the retina. In Neuromethods.
68. Baden, T., Berens, P., Franke, K., Roman-Roson, M., Bethge, M., and Euler (2016). The functional diversity of mouse retinal ganglion cells. Nature, 1–21.
69. Dorostkar, M.M., Dreosti, E., Odermatt, B., and Lagnado, L. (2010). Computational processing of optical measurements of neuronal and synaptic activity in networks. J. Neurosci. Methods *188*, 141–50.